Journal of Constructional Steel Research 189 (2022) 107108

Contents lists available at ScienceDirect

Journal of Constructional Steel Research

journal homepage: www.elsevier.com/locate/jcsr

Probabilistic modelling of residual stresses in cold-formed rectangular hollow sections

Lauri Jaamala *, Kristo Mela, Jussi Laurila, Milla Rinne, Pasi Peura

Tampere University, Tekniikankatu 12, 33720 Tampere, Finland

ARTICLE INFO

Keywords:
Residual stress
Cold-formed
Hollow section
High-strength steel
Experimental investigation
Reliability study

ABSTRACT

This study revisits residual stress models of cold-formed rectangular hollow sections (CFRHS). Residual stresses of CFRHS have a complex distribution that varies along the cross-sectional perimeter and through the material thickness. The distribution depends on the manufacturing methods and steel grades, which constantly evolve. Existing residual stress models are based on old measurements and for normal strength steel specimens (nominal yield strength $f_{y,nom} \leq 460$ MPa). This study evaluates the suitability of these models for modern CFRHS made of normal- and high-strength ($f_{y,nom} > 460$ MPa) steels. Evaluation is carried out as an extensive analysis for a data set, which is collected from the literature, and supplemented with new measurements made for grade S700 specimens. As a result of the evaluation, an updated residual stress model is proposed, which combines the best suitable features of the existing models with slight modifications. The proposed model is valid for CFRHS made of steel grades up to S960. The model can be used in the advanced analyses of CFRHS structures. Additionally, statistical information is provided for the residual stress components such that the model can be used in probabilistic modelling and reliability studies.

1. Introduction

Residual stresses can have a significant impact on the global buckling capacity of the compressed steel members [1]. In advanced design and analysis methods, such as in **G**eometrically and **M**aterially **N**onlinear **I**mperfection **A**nalysis (GMNIA) of EN 1993 [2], residual stress models are needed for two purposes: (1) To incorporate residual stresses into the calculation model when designing with such a method. (2) Additionally, for developing these methods, a statistical residual stress model is needed in determining the partial factors by structural reliability theory, such as in [3].

Residual stresses of CFRHS made of normal-strength steel (NSS, nominal yield strength $f_{y,nom} \leq 460$ MPa) have been extensively studied, and various residual stress models have been proposed such as those by Davison and Birkemoe (model DB) [4] in 1983 and Key and Hancock (model KH) [5] in 1993. CFRHS have complex residual stress distribution that varies along the cross-section perimeter and through the material thickness, and models DB and KH consider these issues. More recent residual stress models have been presented both for NSS and High-strength steel (HSS, $f_{y,nom} > 460$ MPa), for example, by Tong et al. [6] (2012) and Somodi and Kövesdi [7] (2017). Unfortunately, these models do not present residual stresses in sufficient detail for reliability studies, because they do not consider statistical properties and longitudinal membrane or transversal stress components.

HSS differs from NSS in the stress-strain behaviour: NSS has a sharp yield point and can be modelled as a bilinear stress-strain curve [8], whereas HSS has a rounded curve without a clear yield point. Ramberg-Osgood model [9] is typically used to describe the stress-strain curve for HSS [10]. A recent study by Somodi and Kövesdi [7] suggests that the magnitude of the residual stresses in CFRHS does not increase linearly with yield strength. Columns made of HSS seem to have a more beneficial residual stress distribution compared to the yield strength than their NSS counterparts, which in turn favours the buckling capacity of HSS columns [11–14]. Consequently, it is not evident whether the residual stress models developed for NSS are suitable for HSS cold-formed hollow sections.

In this study, the applicability of the models DB and KH for CFRHS members made of HSS is evaluated. New measurements are conducted in this study for specimens made of steel grade S700 to supplement the data found in the literature [6,7,15–25]. This data set including the new measurements is analyzed in the evaluation. In addition to HSS, measurements considering NSS members are included in the data set. This

* Corresponding author.
E-mail address: lauri.jaamala@tuni.fi (L. Jaamala).

https://doi.org/10.1016/j.jcsr.2021.107108
Received 24 September 2021; Received in revised form 29 November 2021; Accepted 16 December 2021
Available online 29 December 2021

inclusion is made to obtain more data samples for the analysis and to simultaneously reassess the applicability of the models DB and KH to modern NSS members. Residual stress distribution highly depends on the manufacturing details and steel grades which constantly evolve. Therefore, modern CFRHS members may not have the same residual stress properties as before.

The evaluation is carried out by analysing the distribution and magnitude of the longitudinal and transversal residual stress components. Curve fitting techniques are employed to determine the magnitude of the components as functions of yield strength. Statistical analysis is then performed for obtaining the probability distributions of the stress components for reliability studies. A new model is proposed that combines the most suitable features of models DB and KH with slight modifications. Finally, a parametric study is presented, where the proposed model for residual stresses is applied on a steel member in compression.

The paper is organised as follows: Section 2 describes the key features of the residual stresses of CFRHS members and presents the models DB and KH. Section 3 presents the experimental part of this study. Results of the experiments together with the data set found from the literature are evaluated in Section 4, where a new updated residual stress model is proposed. Development of the proposed model involves simplifications, and their effects are evaluated for the global buckling capacity in Section 5. Section 6 concludes the study.

2. Residual stresses in cold-formed rectangular hollow sections

Residual stresses are induced to structural members in the fabrication process. The fabrication methods of CFRHS members can be divided into “direct-forming” and “continuous-forming” [17], and induced residual stress distribution between these methods vary [6,15,17]. This study considers only cold-formed members made by the continuous forming method.

Residual stresses in CFRHS are usually divided into longitudinal (σ_L) and transversal (σ_T) components as shown in Fig. 1. σ_L acts along the longitudinal axis of the member and σ_T in the plane of the cross-section. Normal stress σ_z in the through-thickness direction and all shear stresses τ_{xy}, τ_{xz} and τ_{yz} are usually assumed to be negligible. A special characteristic in residual stresses of CFRHS is that the stress distribution varies both along the cross-section perimeter and through the material thickness. Longitudinal and transversal components can be further divided into the longitudinal membrane (σ_{LM}), longitudinal bending (σ_{LB}), transversal membrane (σ_{TM}) and transversal bending (σ_{TB}) components. The total in-situ state of residual stresses through the thickness is obtained by combining membrane and bending components. In the literature, varying shapes have been used to model the longitudinal through-thickness bending component, such as linear, nonlinear, symmetric and unsymmetric distributions [4–7]. Relative longitudinal residual stress distributions are presented in Fig. 2 for the models DB and KH. Both models assume nonlinear through-thickness distribution for longitudinal bending component, DB being symmetric and KH nonsymmetric about the mid-thickness. The longitudinal membrane stress component is uniformly distributed through the thickness in both models. Through-thickness distributions differ remarkably between models DB and KH. These models are based on a few measured specimens, and as presented later in this study, the residual stress distribution has a high variation among individual members. Therefore, differences between models are expected, which in turn also emphasizes the need for a statistical model that is based on multiple measured specimens.

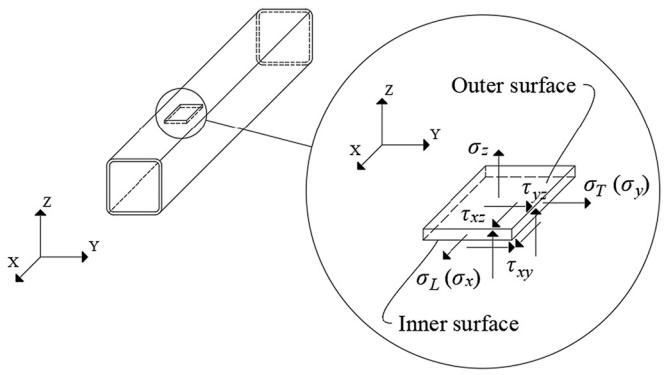

Fig. 1. Residual stress components and their directions in CFRHS.

To consider the variation of residual stresses along the cross-section perimeter, four key locations for each 1/8th of the cross-section are identified as shown in Fig. 3: MP (mid-plate), QP (quarter plate), NC (near corner), and CC (centre of corner). The variation is modelled with the distribution factor χ, which is presented for longitudinal components in Fig. 4. Models assume that the distribution is symmetrical for every 1/8th of the cross-section (from CC to MP) about axes 1–1 and 2–2, see Fig. 3. The membrane component χ_{LM} of both models varies linearly and it is positive (tensile) at MP. The longitudinal bending component χ_{LB} is assumed to be uniformly distributed in both models, but in KH the magnitude in the corner region is half of the magnitude in the flat region.

The DB-model does not consider transversal residual stresses, hence the transversal bending component is presented in Fig. 5 for the KH-model only. The transversal membrane component is assumed to be zero in the KH-model, $\sigma_{TM} = 0$.

Total residual stresses at the location s along the perimeter (see Fig. 3) are obtained by:

$$\sigma_L(s) = \chi_{LM}(s) \bullet \sigma_{LM} + \chi_{LB}(s) \bullet \sigma_{LB} \tag{1}$$

$$\sigma_T(s) = \chi_{TB}(s) \bullet \sigma_{TB} \tag{2}$$

3. Experimental study

Residual stress measurements were carried out by the X-ray diffraction method [26]. The method is rather fast and enables measurements both in the longitudinal and transversal directions.

3.1. Test specimens

Two CFRHS members were studied: rectangular profile (RE) 150x100x6 mm (width (W) x height (H) x thickness (t)) and square profile (SQ) 100x100x6 mm. Both members were split into four separate specimens (RE1-RE4 and SQ1-SQ4) each having a length of 400 mm. The members were manufactured from steel grade S700 and with the same technology. Residual stresses were measured at the outer surface for three of the specimens of both profiles. These measurements were carried out at locations P01-P12 for RE and P02-P06 and P08-P12 for SQ (Fig. 3). The fourth specimens were used to measure the stress distribution through the material thickness at the locations P03, P04, P09 and P10. Tensile strength tests were conducted for two flat test bars of both profiles according to EN ISO 6892-1 [27], and the measured 0.2% proof stresses were 792 MPa and 770 MPa for rectangular and 775 MPa and 777 MPa for square profiles.

3.2. Measuring method

The equipment used to measure the residual stress was ‘XStress 3000’ manufactured by Stresstech Oy Finland. Before the through-thickness measurements, material was removed from the measurement locations by electrochemically polishing with Movipol 5 equipment. Electrochemical polishing is one of the gentlest methods to remove material layers without disturbing the existing residual stress state in the sample [28]. The polishing was carried out using Struers A2 electrolyte (a mixture of 60% perchloric acid, 65–85% ethanol, 10–15% 2-butoxyethanol, and 5–15% water). The measurement results were analyzed with

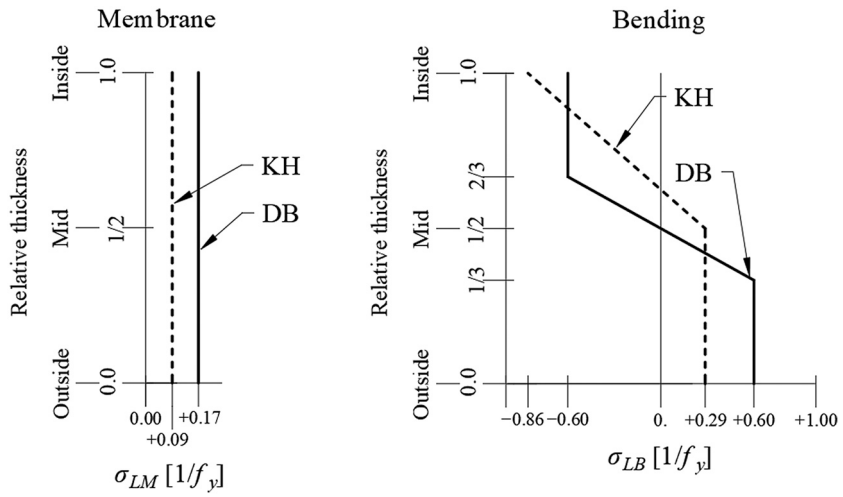

Fig. 2. Through-thickness distributions of longitudinal bending and membrane components relative to the yield strength.

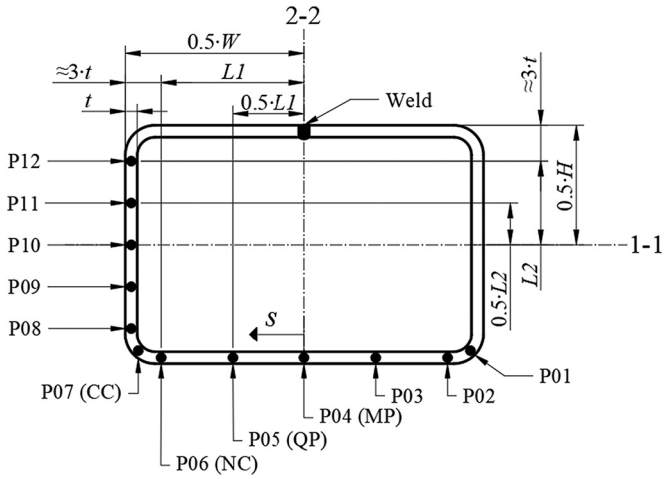

Fig. 3. Relative locations of MP, QP, NC and CC along cross-section perimeter and locations of measurement points P01-P12 for experimental study.

XTronic software. The modified Chi method [29], based on Bragg's law [30], was employed for measuring. Residual stresses were calculated with the parameters shown in Table 1 [31].

Because the polishing method was slow in removing material, the through-thickness stresses were measured from the hollow bottoms, which were machined with a sharp cutter tool to depths of 1, 2, 3 and 4 mm from the profile surface. The machined hollow bottoms were electropolished by a layer thickness of 150–250 μm before measurements. To evaluate the validity of the through-thickness measurement method, stresses were also measured without machining. These results are compared to the used method (machining + gently polishing) in Fig. 6. Close agreement between the measurements suggests that machining does not interfere with the measurements.

3.3. Results of experimental study

Results of the outer surface measurements are shown in Table 2 and Figs. 7(a)-(d). Measurements of all three specimens within the same rectangle or square profile are in close agreement with each other in longitudinal and transversal directions. This observation indicates that results measured only at one longitudinal location of a specimen can be held representative for the whole specimen. Additionally, the observation supports the concept that a constant residual stress model is valid along the axis of a hollow section member as assumed in models DB and KH. The through-thickness measurements are shown in Table 3 and Figs. 8(a)-(d). The square profile has more identical through-thickness distributions within the measurement locations than the rectangular profile.

4. Evaluation of residual stress models

Evaluation of the models DB and KH is carried out separately for the longitudinal bending, longitudinal membrane, and transversal bending

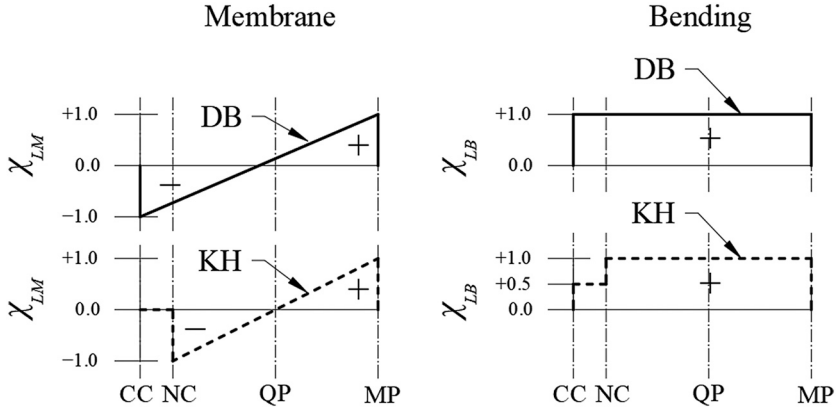

Fig. 4. Distribution factors χ of models DB and KH for longitudinal components along 1/8th cross-section perimeter.

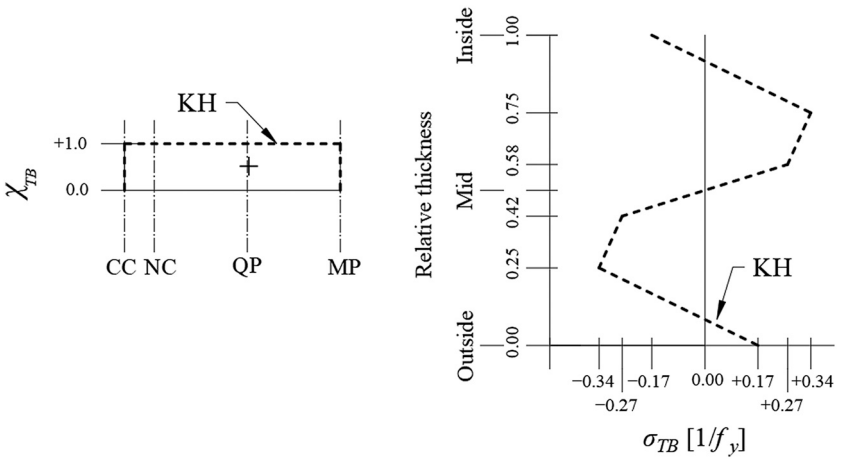

Fig. 5. Distribution factor χ_{TB} along 1/8th cross-section perimeter and relative through-thickness distribution for transversal bending component in model KH.

Table 1
Residual stress measurement parameters.

Measurement directions	0° (σ_L) and 90° (σ_T)
Number of tilt angles ψ	5/5
Maximum tilt angle ψ	±45°
ψ oscillation	5°
Elastic modulus E	211,000 MPa
Poisson's ratio ν	0.3
Voltage	30 kV
Radiation	CrKα

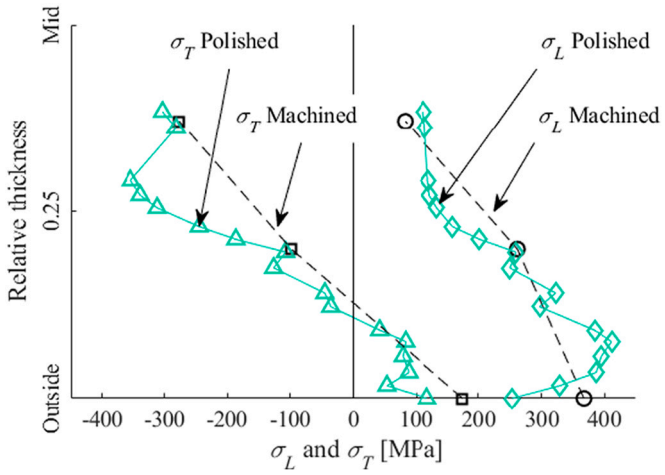

Fig. 6. Comparison of the SQ1-P03 and SQ4-P03 results obtained by machining (used method) and polishing.

components. The evaluation procedure for each component focuses on the following four main characteristics:

1. Suitability of the χ-distribution of Figs. 4 or 5 is evaluated.
2. Average magnitude of the component at the surfaces of the cross-section is determined.
3. Statistical properties of the average magnitude of the component are determined in the form of an error term.
4. In the case of the bending component, the suitability of the through-thickness distribution of Figs. 2 or 5 is evaluated.

Based on the evaluation, an updated model for residual stresses of cold-formed rectangular hollow sections is presented.

4.1. Collected data from the literature

A data set of measurements consisting of 49 specimens is gathered from the literature, and relevant information of these tests is shown in Table 4. Only tests conducted on continuous-formed members and published after models DB and KH were included, thus focusing on modern sections, and excluding measurements related to models DB and KH from the compared data set. The measurements presented in Section 3 are added to the data set as specimens RE and SQ having the mean values of the surface measurements RE1-RE3 for rectangular and SQ1-SQ3 for square cross-section (see Fig. 7).

Measurements of the data set were carried out with various methods. It is worth noting that different methods and different approaches within the same method can lead to differing residual stress measurements. For example, some studies presented in Table 4 use the sectioning method such that residual stresses are determined from the curvature and elongation of the sectioned coupons by measuring geometrical dimensions, whereas some studies measure stresses from strain gauge readings. These two approaches have different measurement accuracy. Additionally, because the sectioning method measures residual stresses from the released coupon, the whole through-thickness residual stress state affects deformations and subsequently to measured stresses of the released coupon. The X-ray diffraction or hole-drilling method on the other hand results in a more local stress reading. Because this study combines the measurements obtained using various methods, the measuring differences will be inevitably included in a statistical dispersion of the proposed model.

To generate more consistent measurements, in this study, the results of Sun and Packer [17] have been scaled up such that the procedure corresponds to the sectioning method used by Somodi and Kövesdi and Ma et al. Sun and Packer considered the residual stress state of the sectioned coupon, which is not free from stresses, by scaling down the measured surface stresses. Additionally, they reported the results relative to compressive rather than tensile yield strength. Scaling up the measurements of Sun and Packer increases stresses, but this procedure is conservative because residual stresses are usually unfavourable for member capacities. In addition, Gardner et al. [16] used the sectioning method such that only the longitudinal bending component was measured. Hence, these measurements have been included in the data set only when studying the bending residual stresses.

The magnitude of residual stresses depends on the yield stress [7]. Therefore, throughout this evaluation, residual stresses are expressed relative to the (measured) tensile yield stress f_y of the flat region shown in Table 4. HSS do not have a clear yield point, hence f_y of HSS refers to the 0.2% tensile proof stress of the flat region.

It should be noted that the longitudinal welding of CFRHS affects the

Table 2
Measured residual stresses at the outer surface.

Point	Specimen / Component [MPa]											
	RE1		RE2		RE3		SQ1		SQ2		SQ3	
	σ_L	σ_T	σ_L	σ_T	σ_L	σ_T	σ_L	σ_T	σ_L	σ_T	σ_L	σ_T
P01	198	77	223	35	249	142	–	–	–	–	–	–
P02	204	−90	270	−15	281	12	345	−85	241	−169	267	−253
P03	309	288	230	173	307	251	254	118	337	181	350	174
P04	62	−47	36	−25	204	103	157	8	68	−48	88	−30
P05	308	259	286	274	318	284	392	151	301	94	325	180
P06	327	−38	148	−168	296	−111	234	−250	248	−282	353	−153
P07	216	59	180	48	253	112	–	–	–	–	–	–
P08	376	52	157	−39	182	56	11	−352	−2	−202	−30	−249
P09	328	152	348	137	338	154	285	184	282	158	290	183
P10	274	175	286	173	274	178	270	152	140	32	176	69
P11	348	160	332	160	316	171	289	118	311	182	262	164
P12	73	76	55	25	−30	63	43	−219	−53	−233	−51	−230

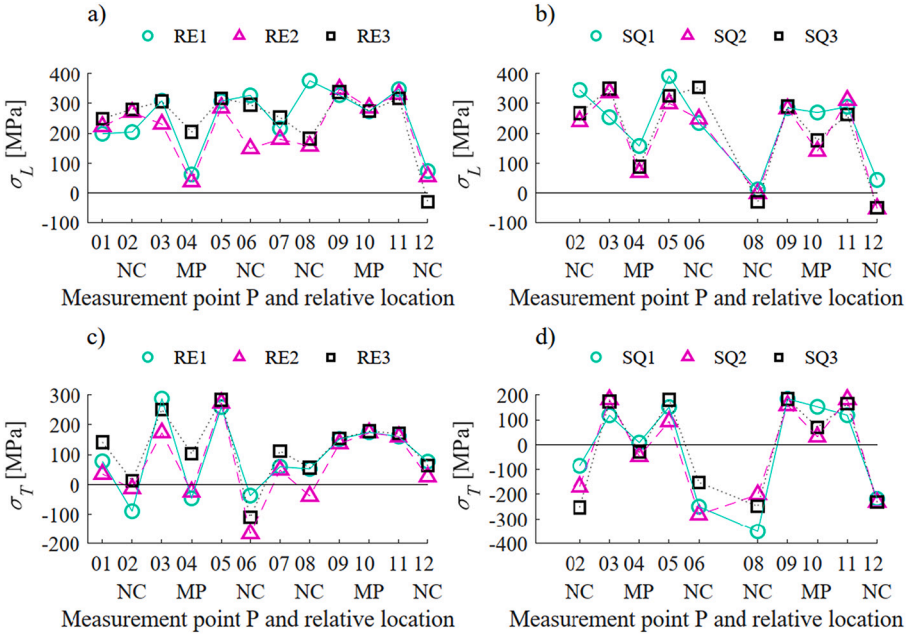

Fig. 7. Results of the outer surface measurements.

residual stresses near the weld. However, the heat-affected zone is minor compared to the cross-sectional area so the overall effect of the weld to member capacity is assumed to be insignificant. Measurements are analyzed for every 1/8th cross-section face between CC and MP (see Fig. 3) in this study. Consequently, any measurements from the faces containing the longitudinal weld are excluded from the data set.

4.2. Longitudinal residual stresses

Relative longitudinal residual stresses σ_L from the data set (see Table 4) at outer and inner surfaces (see Fig. 1) of a cross-section are presented in Fig. 9. The data set consists a total of 697 outer and 522 inner surface measurements. However, most of the inner surface measurements presented in Fig. 9 are not the actual readings from the inner surface of the specimens. In many studies, the sectioning method is used without strain gauges such that residual stresses at the surfaces are determined from the average curvature and elongation of the sectioned coupons. Hence, this approach does not directly measure the inner surface, and the data set consisted only of 133 actual inner surface measurements. Each connecting line represents 1/8th of a cross-section for a given specimen of the data set. The data of Fig. 9 illustrates the well-known observation that longitudinal residual stresses are tensile (positive) at the outer surface and compressive (negative) at the inner surface. However, for a few measurements, the outer surface is in compression and the inner surface in tension. Somodi and Kövesdi [7] noticed that the stress difference between NC and MP depends on the B/t-ratio. According to outer surface measurements, the stress difference between NC and MP of the flat faces has a moderate linear correlation with B/t-ratio, having Pearson's coefficient of 0.57. With increasing B/t-ratio the stress level at NC in relation to MP increases. Thus, B/t-ratio affects the shape of the σ_L distribution. However, a linear correlation between the stress difference and yield stress was not observed.

4.2.1. χ_{LB} for longitudinal bending component

The distribution of χ_{LB} is determined from the variation of σ_{LB} along the cross-section perimeter. According to Fig. 9, the connecting lines of different 1/8th faces are entangled without a clear trend, i.e. variation is considerable. Therefore, developing a general model for χ_{LB} inevitably leads to gross simplifications, which in turn encourages choosing some simple distribution. Fig. 10(a) presents regression lines of the longitudinal flat region measurements. Grouping according to the B/t-ratio shows how the ratio affects the shape of the χ_{LB} distribution. The limits for the B/t-ratio are determined such that every group contains approximately the same number of specimens. Regression lines contain

Table 3
Measured through-thickness residual stresses of sections RE4 and SQ4.

Point	Rectangular section RE4			Square section SQ4		
	Depth [mm]	σ_L [MPa]	σ_T [MPa]	Depth [mm]	σ_L [MPa]	σ_T [MPa]
	0	228	215	0	368	175
	1.20	147	10	1.20	262	−98
P03	2.21	125	−207	2.23	83	−276
	3.25	221	−133	3.24	85	−105
	4.21	217	316	4.20	62	248
	0	−94	−115	0	182	54
	1.20	265	−17	1.31	148	−218
P04	2.20	255	−140	2.20	153	−310
	3.23	289	11	3.23	190	43
	4.19	140	282	4.20	196	407
	0	380	103	0	372	149
	1.31	416	150	1.20	249	−26
P09	2.30	14	−60	2.19	4	−261
	3.19	−70	−161	3.20	−31	−249
	4.29	−311	120	4.26	−35	297
	0	298	145	0	269	116
	1.22	182	110	1.25	157	−100
P10	2.23	−61	−191	2.27	67	−292
	3.22	−96	−254	3.20	190	−136
	4.27	−231	226	4.20	157	292

the effects of both the bending and the membrane components. The bending component can be distinguished from the outer and inner surface measurements by the equation $\sigma_{LB} = (\sigma_{L,Outer\ surface} - \sigma_{L,\ Inner\ surface})\ /\ 2$ as in [18]. Employing this equation for the regression lines of Fig. 10 (a), the lines presented in Fig. 10(b) are obtained. The negative slopes show that the average σ_{LB} increases from MP to NC in every B/t-ratio group. The maximum increase is 66% in the case of $30 \leq B/t$, and 33% on average for "All". Because the increase of σ_{LB} seems minor on average, and the general model for χ_{LB} is a gross simplification in any case, it seems reasonable to use uniform distribution as in models DB and KH (Fig. 4). Effects of horizontal vs. descending χ_{LB} on the buckling capacity are explored in Section 5.

According to Fig. 9, a sudden change in the residual stress magnitudes can be observed between NC and CC in many cases. This encourages to use the distribution χ_{LB} of model KH over DB such that the differences between corner and flat regions are distinguished.

4.2.2. *Magnitude σ_{LB} for longitudinal bending component*

For the magnitude of the longitudinal bending component, σ_{LB}, the DB suggests ± 0.6 for both outer and inner surfaces, whereas KH suggests $+0.29$ for outer and -0.86 for inner surfaces (see Fig. 2). The models DB and KH were created for specimens with measured yield strengths between 250 and 500 MPa so they were not based on HSS sections. Somodi and Kövesdi [7] suggested that the magnitude of residual stresses depends on the yield stress. They developed two equations to calculate the magnitude of σ_{LB} for NSS and HSS, which are plotted in Fig. 11.

Fig. 11 contains data points for the average longitudinal outer surface residual stresses for every 1/8th flat face between MP and NC. Average magnitudes of the longitudinal bending component were determined by the formula:

$$\sigma_{L,Avg,Flat} = \frac{\int_{s_{MP}}^{s_{NC}} \left|\sigma_L(s)\right| ds}{\int_{s_{MP}}^{s_{NC}} ds} = \frac{\int_{s_{MP}}^{s_{NC}} \left|\sigma_{LB}(s) + \sigma_{LM}(s)\right| ds}{\int_{s_{MP}}^{s_{NC}} ds} \tag{3}$$

where s_{MP} and s_{NC} are the local coordinates at MP and NC along the perimeter of the cross-section (Fig. 3). Note that the absolute value of the stress is used in the integration because in some cases, compressive residual stresses at parts of the outer surface were reported. It is assumed

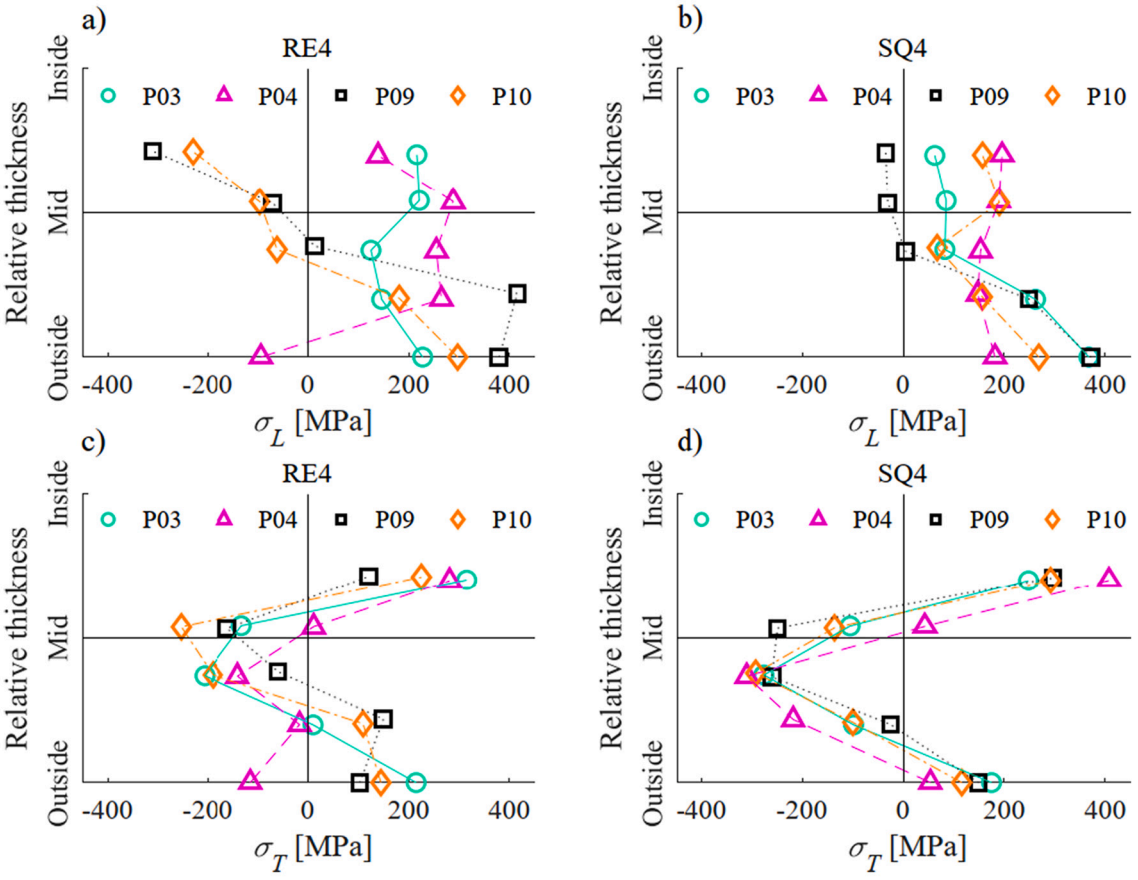

Fig. 8. Results of the through-thickness measurements.

Table 4
Data set for evaluation of residual stresses.

Authors	Specimen name	Meas. method	$f_{y,nom}$ [MPa]	f_y [MPa]	W [mm]	H [mm]	t [mm]	B/t
Somodi, Kövesdi [7]	CF4.2-100x3_R	Sectioning	420	458	100	100	3	33.3
	CF4.2-120x6_R	Sectioning	420	506	120	120	6	20.0
	CF4.2-150x5_R	Sectioning	420	479	150	150	5	30.0
	CF4.6-150x8_R	Sectioning	460	508	150	150	8	18.8
	CF4.6-120x4_R	Sectioning	460	559	120	120	4	30.0
	CF5-120x6_V	Sectioning	500	624	120	120	6	20.0
	CF5-130x4_V	Sectioning	500	573	130	130	4	32.5
	CF5-200x5_V	Sectioning	500	567	200	200	5	40.0
	CF7–150x4_V	Sectioning	700	799	150	150	4	37.5
	CF7–150x8_R	Sectioning	700	742	150	150	8	18.8
	CF9–120x4_R	Sectioning	960	1049	120	120	4	30.0
	CF9–120x6_R	Sectioning	960	1088	120	120	6	20.0
	CF9–150x7_R	Sectioning	960	1114	150	150	7.1	21.1
Sun, Packer [17]	CF1	Sectioning	350	457	152	152	12.7	12.0
	CF3	Sectioning	350	330	152	152	6.35	23.9
Li S.H. et al. [15]	B	X-ray	NA	266	135	135	12	11.3
	C	X-ray	NA	248	135	135	10	13.5
	F	X-ray	NA	246	200	200	5	40.0
Tong et al. [6]	C135x10	Hole-drilling	NA	391	135	135	10	13.5
Ma et al. [18]	H200x120x5	Sectioning	700	738	200	120	5	40.0, 24.0
	V120x120x4	Sectioning	900	960	120	120	4	30.0
Gardner et al. [16]	100x100x4-CF	Sectioning	235	482	100	100	4	25.0
	60x60x3-CF	Sectioning	235	361	60	60	3	20.0
	60x40x4-CF	Sectioning	235	400	60	40	4	15.0, 10.0
	40x40x4-CF	Sectioning	235	410	40	40	4	10.0
	40x40x3-CF	Sectioning	235	451	40	40	3	13.3
Zhang et al. [19]	Cold-formed	Hole-drilling	350	521	200	200	12.5	16.0
Sun, Ma [20]	8-C-U	Hole-drilling	350	458	102	102	7.9	12.9
	13-C-U	Hole-drilling	350	483	102	102	13	7.8
Sully, Hancock [21]	125x125x6 SHS	Sectioning	NA	383	125	125	6	20.8
Sun et al. [22]	100x100x8 SHS	Sectioning	NA	370	100	100	8	12.5
Li G.W. et al. [23]	S1	Sectioning	235	299	135	135	10	13.5
	S2	Sectioning	235	389	135	135	12	11.3
	S3	Sectioning	345	425	86	86	8	10.8
	R4	Sectioning	345	416	160	80	8	20.0, 10.0
	S5	Sectioning	345	381	220	220	10	22.0
	S6	Sectioning	345	362	250	250	8	31.3
	S7–1	Sectioning	345	511	108	108	10	10.8
	S8–1	Sectioning	345	391	135	135	10	13.5
	S9–1	Sectioning	345	395	250	250	8	31.3
	S10–1	Sectioning	345	455	350	350	12	29.2
	R11–1	Sectioning	345	368	400	200	10	40.0, 20.0
Tayyebi et al. [24]	I-102x102x6.4-U	Sectioning	350	415	102	102	6.4	15.9
	I-102x102x7.9-U	Sectioning	350	458	102	102	7.9	12.9
	I-102x102x13-U	Sectioning	350	483	102	102	13	7.8
Hayeck [25]	CF 220x120x6	Sectioning	355	453	220	120	6	36.7, 20.0
	CF 200x100x4	Sectioning	355	468	200	100	4	50.0, 25.0
Current study	RE	X-ray	700	781	150	100	6	25.0, 16.7
	SQ	X-ray	700	776	100	100	6	16.7

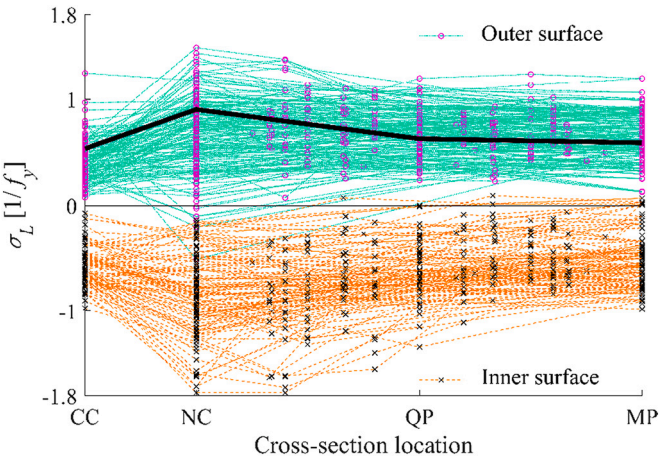

Fig. 9. Longitudinal stress measurements at surfaces (one o.s. 1/8th face highlighted with thick solid line).

that the average stress $\sigma_{L,\,Avg,\,Flat}$ directly represents the magnitudes of the bending component σ_{LB} at the outer surface, although the measurements contain the effects of both bending and membrane components. This assumption is justified since the membrane stress resultant (approximately) vanishes in the integration over the cross-section perimeter.

By fitting a second-order polynomial to the average stresses the following equation is obtained:

$$\sigma_{LB,\mu,Flat}(f_y) = -7.694 \bullet 10^{-7} \bullet f_y^{\,2} + 6.737 \bullet 10^{-4} \bullet f_y + 0.562 \quad [1/f_y] \qquad (4)$$

where f_y is the yield stress of the flat region in MPa. Eq. (4) is plotted in Fig. 11, and it models the mean residual stress level σ_{LB} at surfaces. Eq. (4) is continuous over the entire range of yield stresses, which is convenient in reliability studies, where the yield stress and consequently residual stresses are sampled from statistical distributions. Eq. (4) has been derived in relative residual stress space. If the polynomial is fitted in real stress space, the curve $\sigma_{LB,s\text{-}space}$ shown as a dotted line in Fig. 11 is obtained. This curve differs slightly from $\sigma_{LB,\mu,Flat}$.

The mean of the data points in Fig. 11 is 0.68 and the coefficient of variation is 0.33. By comparing the model of Eq. (4) to the imaginary

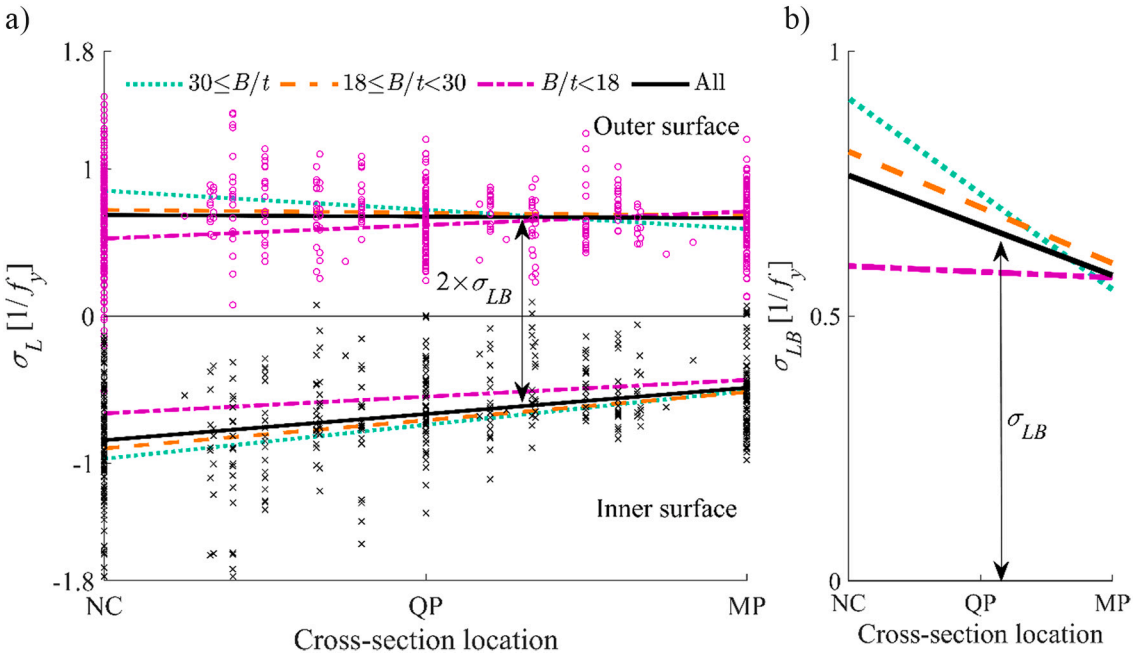

Fig. 10. Regression lines for outer and inner surface measurements (a) and their mean curves of the absolute values (b).

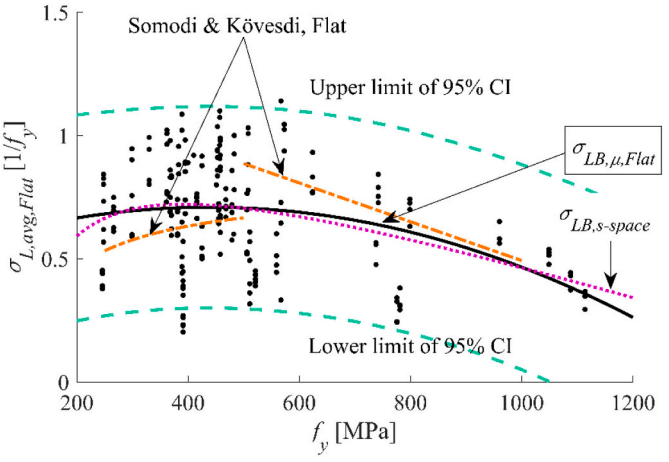

Fig. 11. Average longitudinal residual stresses at the outer surface in the function of yield stress and polynomial fit $\sigma_{LB,\mu,Flat}$.

horizontal line located at the mean value of 0.68, the coefficient of determination (R^2) of 0.12 can be obtained. This means that Eq. (4) models the variation of residual stress magnitude slightly better than the imagined horizontal line. In addition to the yield stress, Li G. [23] determined that the other explanatory variables for the residual stress distribution are the material thickness, width-to-thickness ratio, width-to-corner radius ratio and ultimate-to-tensile strength ratio. Consideration of these variables could enhance the accuracy of the model, but the inclusion of these variables in practical design can be challenging. Additionally, many studies of the data set do not contain sufficient information on these variables. Therefore, the yield stress is chosen as the only explanatory variable in this study.

It should be noted that although the distribution of χ_{LB} correlated with the B/t-ratio, no correlation was found for the magnitude of $\sigma_{L,Avg,Flat}$ and B/t-ratio. The data set contained 6 rectangular specimens from which multiple measurements had been taken from flanges and webs. The width-to-height ratios of these specimens varied between 1.5:1 and 2:1. Longitudinal outer surface residual stress distributions of the specimens were quite identical among all sides, but shorter sides had about 10% higher longitudinal bending residual stress level on average than longer sides. No remarkable difference was observed when comparing the distributions of the rectangular sections to the suggested model. This indicates that residual stresses of rectangular sections do not have to treat separately from square sections. However, the amount of data considering measurements of the rectangular sections was insufficient to make comprehensive conclusions.

The average compressive stresses of the inner surface are presented as data points in Fig. 12. These stresses are calculated by Eq. (3) and presented with a negative sign. Only the actual inner surface measurements were included in this data group (see Section 4.2). By fitting a second-order polynomial to these points, the curve $\sigma_{LB,Flat,In}$ is obtained. The outer surface curve $\sigma_{LB,\mu,Flat}$ is mirrored along the horizontal axis and presented as dotted line $\sigma_{LB,\mu,Flat,Mir}$ in the figure. The curves $\sigma_{LB,\mu,Flat,Mir}$ and $\sigma_{LB,Flat,In}$ provide quite similar stress levels, especially for HSS. Due to the similarity of the curves, it is assumed that the absolute magnitude of longitudinal residual stress both at the outer and inner surface can be modelled with curve $\sigma_{LB,\mu,Flat}$. Curve $\sigma_{LB,\mu,Flat}$ is chosen

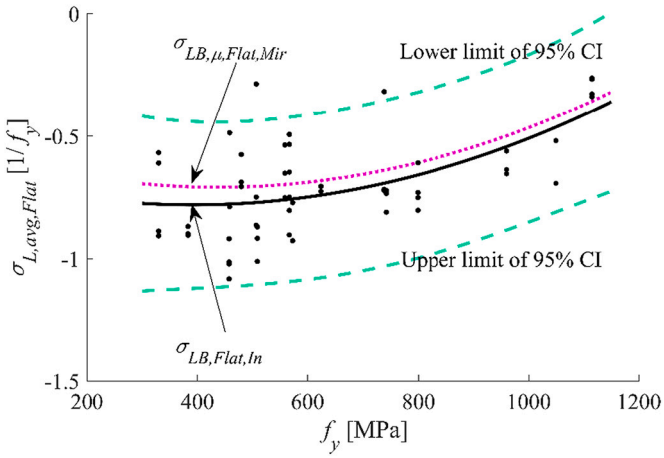

Fig. 12. Average longitudinal residual stresses at the inner surface in the function of yield stress and polynomial fit $\sigma_{LB,Flat,In}$.

over $\sigma_{LB,Flat,In}$ due to larger sample size. The almost equal stress levels between these curves also indicate that the average through-thickness distribution of σ_{LB} is more like DB than KH because of the symmetry (see Fig. 2). In KH, stress levels at the surfaces have significant differences (−0.86 inner vs. +0.29 outer).

Average longitudinal residual stresses of the corner region are shown in Fig. 13. Except for one study, the corner regions contained at most one measurement per corner in every specimen, i.e. no measurements between NC and CC existed. For the experiments having measurements at both NC and CC, the average residual stress in the corner was calculated as the average value of the absolute values of NC and CC. For the specimens with measurement only at CC (and not at NC), the average value was directly taken as the value at CC. In the case of the study that exceptionally contained multiple measurements at the corner area, the measurements of the corner area were first averaged to a single CC value and then treated similarly as in other studies.

By fitting a second-order polynomial to these average stresses the following equation is obtained:

$$\sigma_{LB,\mu,Corner}(f_y) = -4.757 \bullet 10^{-7} \bullet f_y^2 + 2.161 \bullet 10^{-4} \bullet f_y + 0.548 \quad [1/f_y] \tag{5}$$

where f_y is the yield stress of the flat region in MPa. The curves $\sigma_{LB,\mu,Corner}$ and $\sigma_{LB,\mu,Flat}$ are plotted in Fig. 13. Curve $\sigma_{LB,\mu,Corner}$ has a similar trend as $\sigma_{LB,\mu,Flat}$, yielding slightly lower residual stress levels than $\sigma_{LB,\mu,Flat}$. Models of Somodi and Kövesdi [7] assume that σ_{LB} of the corner region is 55% of the residual stress of the flat region. These curves are also plotted, and they provide lower residual stresses for the corner than Eq. (5). The mean of the data points in Fig. 13 is 0.53 and the coefficient of variation is 0.39. The coefficient of determination for the model of Eq. (5) is 0.11, which is approximately the same as for the model $\sigma_{LB,\mu,Flat}$ (0.12).

A strong linear correlation with Pearson's coefficient of 0.80 was found between the average longitudinal bending residual stresses in the corner and flat regions. Because of the strong correlation, the residual stress level at the corner may be modelled to fully correlate with the flat region. The fully correlated stress level at the corner can be obtained by:

$$\sigma_{LB,Corner,Corr}(\sigma_{LB,Flat}) = 0.757 \bullet \sigma_{LB,Flat} + 0.024 \quad [1/f_y] \tag{6}$$

where $\sigma_{LB,Flat}$ is the total relative longitudinal bending residual stress level at flat region. In the sampling of the residual stress values, such as in Monte Carlo simulations, the total residual stress value for a sample can be calculated as:

$$\sigma_{i,j}(f_y) = \sigma_{i,\mu,j}(f_y) + \sigma_{i,\Delta,j} \quad [1/f_y] \tag{7}$$

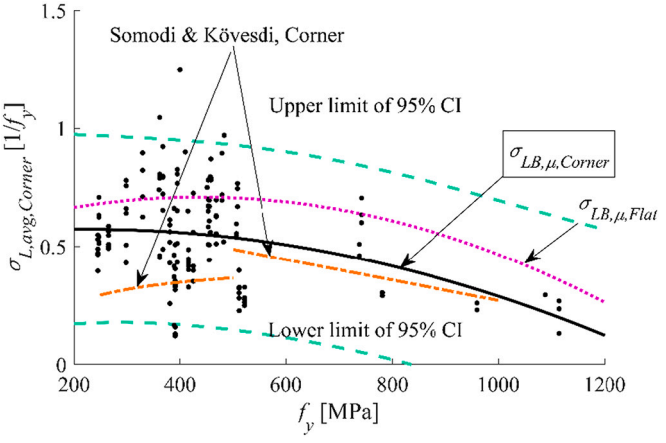

Fig. 13. Average longitudinal residual stresses at the outer surface of the corner region in the function of yield stress and polynomial fit $\sigma_{LB,\mu,Corner}$.

where $i = LM$, LB or TB and $j = Flat$ or $Corner$. The term $\sigma_{i,\mu,j}$ is the mean value of the residual stress level, such as $\sigma_{LB,\mu,Flat}$ according to Eq. (4). The $\sigma_{i,\Delta,j}$ is the sampled error term, which models the variation around the mean μ by statistical properties presented in the following Sections. If the residual stress level at the corner is assumed to fully correlate with the flat region, the stress level at the corner can be calculated using Eq. (6). However, if modelling of dependence between the flat and corner stresses is of interest, dependent samples can be generated with qs. (4 and 5) and the correlation coefficient.

4.2.3. Statistical properties of σ_{LB}

The models for residual stresses derived above represent the mean residual stress levels. In structural reliability analysis, a statistical distribution of residual stresses is needed. The 95% confidence intervals (CI) drawn as dashed lines in Figs. **11** and **13** show that the deviation of average residual stresses around the curves $\sigma_{LB,\mu,Flat}$ and $\sigma_{LB,\mu,Corner}$ is significant. This deviation can be considered in probabilistic modelling by the error term $\sigma_{LB,\Delta,Flat}$ (and $\sigma_{LB,\Delta,Corner}$), which is determined by subtracting the yield-stress-specific model value i.e. the mean value from every measured value. In this study, it is assumed that the distribution of the error term is independent of the yield stress. This assumption may not be entirely accurate in practice, because varying chemical compositions and processing routes are used for commercial steel grades, and these factors affect the magnitude of residual stresses [32,33]. Developing steel grade-specific residual stress models could lead to smaller mean values and deviations of the error term. However, the amount of available data is not sufficient for steel grade-specific statistical models, especially for HSS. Therefore, in this study, a single statistical model for a wide range of steel grades is developed.

Normalized histogram of the error term $\sigma_{LB,\Delta,Flat}$ for the model $\sigma_{LB,Flat}$ is shown in Fig. 14(a) along with probability density functions (PDF) of Kernel Density Estimation (KDE) [34], Normal, and Johnson SB distribution [35]. The sample mean of the error term is 0 and the sample standard deviation (STD) is 0.21. The distribution resembles a reversed Log-normal distribution. This type of distribution can be modelled as bounded Johnson SB, which fits better than Normal to the histogram. Parameters γ, δ, ξ and λ needed for Johnson SB are determined by Matlab toolbox [36] and presented later in Table 5. Empirical, Normal and Johnson SB cumulative distribution functions (CDF) for $\sigma_{LB,\Delta,Flat}$ are shown in Fig. 14(b). Both Normal and Johnson SB follow quite well Empirical CDF, i.e. both distributions seem valid to draw samples. It should be noted that Johnson SB is bounded distribution unlike Normal, i.e. it does not result as extreme values as Normal. In the case of residual stresses, however, stresses are not able to exceed ultimate strength, thus the lack of infinity of the distribution is not crucial.

In the literature, the longitudinal bending component has been modelled with Normal and Log-normal distributions for NSS [37,38], with the mean of 0.7 and the coefficient of variation of 0.05 and 0.07. These values result in even 4–6 times smaller STD's than obtained by the model $\sigma_{LB,Flat}$. In the case of the mean value, however, models result in a higher value than $\sigma_{LB,Flat}$ in general.

Normalized histogram of the error term $\sigma_{LB,\Delta,Corner}$ for the corner model $\sigma_{LB,Corner}$ is shown in Fig. 14(c). Normal distribution can be fitted to the data with parameters $N(0,0.20)$ and Matlab toolbox [36] fits the unbounded Johnson SU distribution with parameters presented later in Table 5. Fig. 14(d) presents CDF's of Empirical, Normal and Johnson SU.

4.2.4. Through-thickness distribution of σ_{LB}

The data set contains a total of 101 through-thickness longitudinal measurements in addition to outer and inner surface measurements, and they are shown in Fig. 15. To increase the sample size, such measurements were also included which were recorded from the corner and near corner regions of the faces containing the longitudinal weld, because welding has no impact on these regions. In addition, each of the four through-thickness patterns measured in this study was considered as an independent sample, even though they were taken only from two

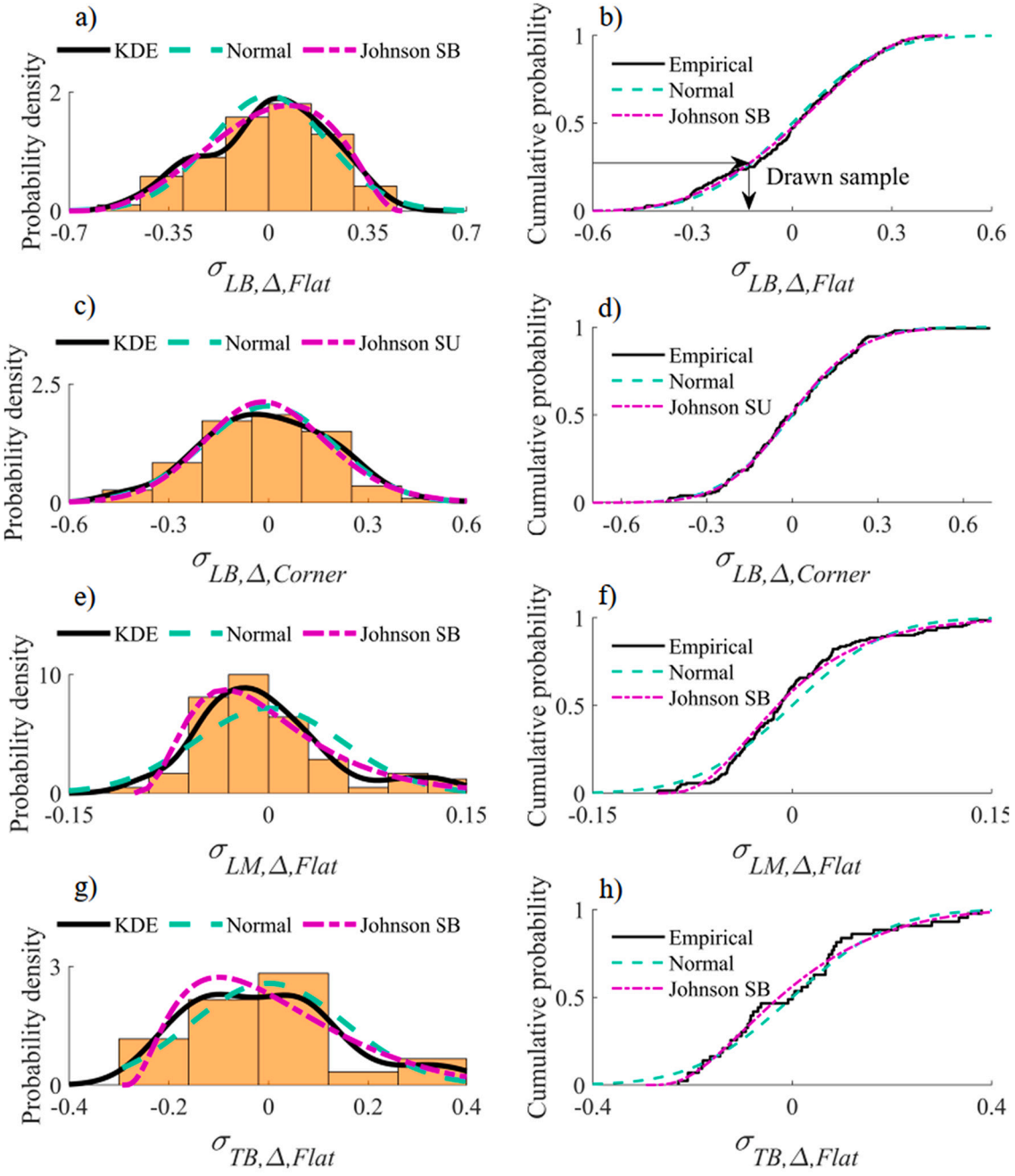

Fig. 14. Histograms, PDF's, and CDF's of the error terms of the residual stress components.

different specimens. It should be noted that all the longitudinal through-thickness bending measurements have been taken only from 5 different specimens, i.e. the sample size is rather low. However, in this study, only minor modifications are made to existing through-thickness models (σ_{LB} and σ_{TB}) without developing new ones. Therefore, small sample sizes in through-thickness measurements are justified.

To study the distribution of the through-thickness stresses at various locations of the cross-section, measurements were grouped to Corner, Near corner, Mid plate, and All. For each of these groups, the residual stresses were approximated by a third-order polynomial as shown in Fig. 16. The through-thickness stresses vary nearly linearly for the flat part of the cross-section (Mid plate). This differs from the Corner and Near corner regions which exhibit more nonlinear behaviour. As the amount of available data is limited, in this study the curve 'All' is taken to represent the distribution of through-thickness stresses.

Measurements in Figs. 15 and 16 contain the effects of membrane residual stresses. The through-thickness membrane component is assumed to be constant as shown in Fig. 2. Consequently, it does not affect the shape of the total through-thickness distribution. In addition, according to the results presented later, the membrane residual stresses are low in general. Hence, it is assumed that the shape of the through-thickness bending component can be determined from the total through-thickness stress distribution, even when it also contains some effects of the membrane component.

The stress distribution provided by the polynomial "All" of Fig. 16 is compared with the models DB and KH in Fig. 17. The distribution "All" agrees better with DB than KH, being nearly symmetrical. In addition, Fig. 17 illustrates the proposed shape for the stress distribution, which is piecewise linear and symmetrical. It is based on the polynomial "Absolute val." which is a third-order approximation of all the

Table 5
Statistics of the proposed probabilistic residual stress model.

Component	Description	Mean [μ]	Parameters for the error term [Δ]	
			Distribution	Parameters around zero mean
$\sigma_{LB,Flat}$	The longitudinal bending in the flat region	Eq. (4)	Normal	Standard dev. $\sigma = 0.206$
			Johnson SB	$\gamma = -0.559$, $\delta = 1.252$ $\xi = -0.721$, $\lambda = 1.208$
$\sigma_{LB,Corner}$	The longitudinal bending in the corner region	Eq. (5)	Normal	Standard dev. $\sigma = 0.196$
			Johnson SU	$\gamma = -0.832$, $\delta = 3.674$ $\xi = -0.160$, $\lambda = 0.674$
		Eq. (6)	No error term, full correlation with $\sigma_{LB,Flat}$	
$\sigma_{LM,Flat}$	The longitudinal membrane in the flat region	Eq. (8)	Normal	Standard dev. $\sigma = 0.056$
			Johnson SB	$\gamma = 3.630$, $\delta = 1.749$ $\xi = -0.111$, $\lambda = 0.895$
$\sigma_{TB,Flat}$	The transversal bending in the flat region	Eq. (9)	Normal	Standard dev. $\sigma = 0.155$
			Johnson SB	$\gamma = 1.267$, $\delta = 1.226$ $\xi = -0.294$, $\lambda = 1.023$
$\sigma_{TB,Corner}$	The transversal bending in the corner region	$= \sigma_{TB,Flat}$		

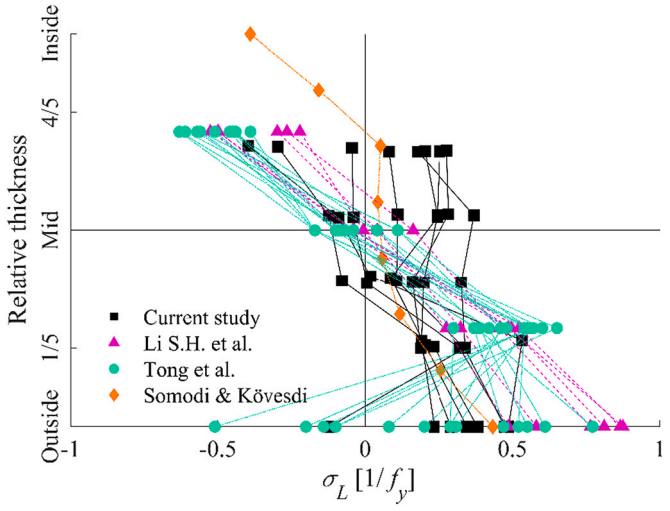

Fig. 15. Internal longitudinal residual stress measurements.

measurements, where the absolute values of outer surface stresses have been employed. This approach is consistent with the method used to determine the means $\sigma_{LM,\mu,Flat}$ and $\sigma_{LM,\mu,Corner}$.

4.2.5. χ_{LM} for longitudinal membrane component

The distribution χ_{LM} is determined from the variation of the longitudinal membrane component σ_{LM} along the cross-section perimeter. σ_{LM} is calculated from the measured residual stresses at the outer and inner surfaces according to the equation $\sigma_{LM} = (\sigma_{L,Outer\ surface} + \sigma_{L,Inner\ surface})\ /\ 2$ such as in [18]. This equation assumes that the bending component causes equal absolute stresses at the outer and inner surfaces such that the equation results in zero in the case of zero membrane stress. According to Fig. 12, the average outer and inner surface stresses are almost equal, i.e. assumption holds approximately true.

The data set consisted of 33 specimens and a total of 522 measurements that contained both the outer and inner surface measurements at the same cross-sectional location. Fig. 18 presents the calculated membrane residual stresses based on these measurements. Connection lines represent 1/8th faces, and no clear trend exists, thus a single universal shape for χ_{LM} inevitably is a gross simplification. Fig. 19 presents the regression lines for the data points of Fig. 18 between NC and MP. The slopes of the regression lines are positive and rather similar despite the B/t-ratio. Consequently, a simple linear distribution such as χ_{LM} of model KH (see Fig. 4) seems reasonable. However, because the slope of χ_{LM} for an individual specimen can also be negative, the sensitivity of the results to the sign of the slope is evaluated in the parametric study.

The membrane component is assumed to be zero in the corner region in the adopted χ_{LM} of model KH. This assumption is justified since

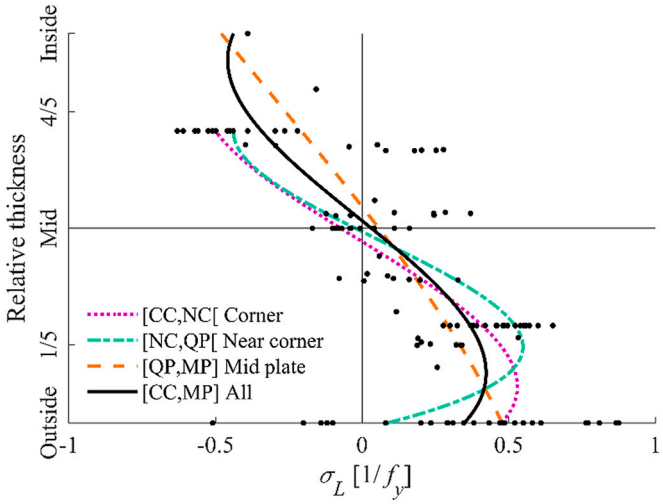

Fig. 16. Through-thickness shapes of σ_L at the regions of corner, near corner, mid plate, and All.

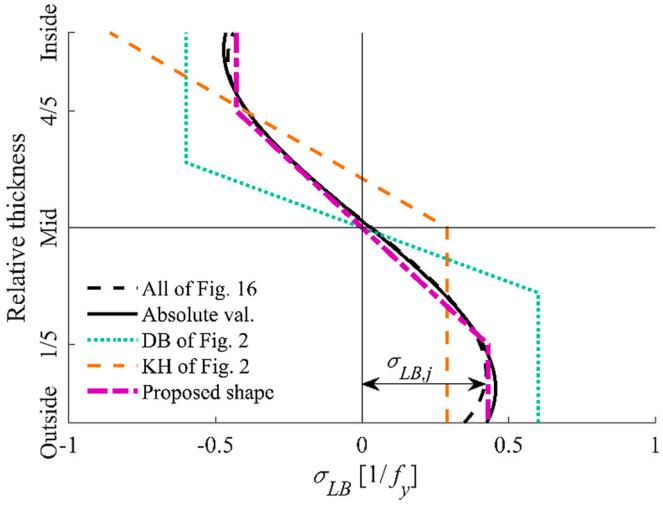

Fig. 17. Comparison of through-thickness shapes for σ_{LB}.

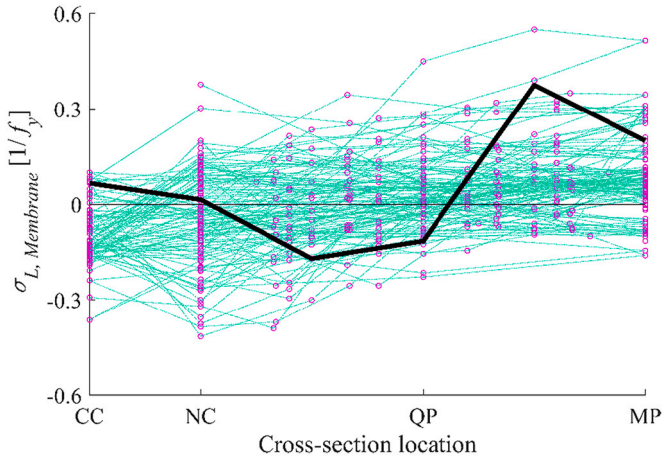

Fig. 18. Longitudinal membrane residual stresses $\sigma_{L,Membrane}$ calculated from the outer and inner surface measurements. (one 1/8th face highlighted).

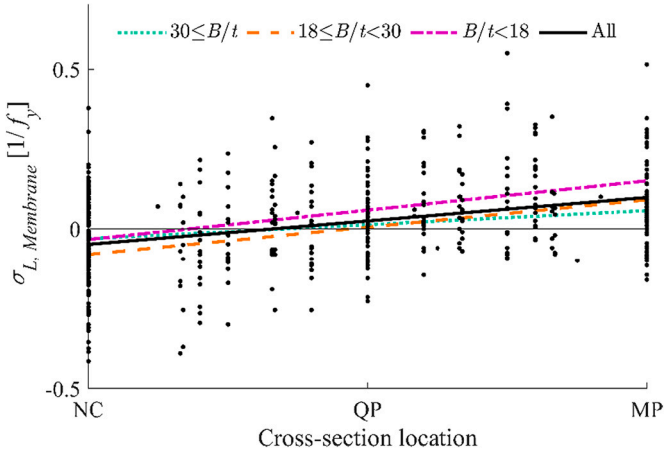

Fig. 19. Regression lines for longitudinal membrane residual stresses grouped by B/t-ratio.

according to Davison and Birkemoe [4], the membrane component has only a minor effect on the global buckling capacity. In addition, the corner region represents a quite limited area of the whole cross-section. Hence, it is assumed that the σ_{LM} in the corner has a negligible effect on column strength and can be omitted.

4.2.6. Magnitude σ_{LM} for longitudinal membrane component

Average longitudinal membrane residual stresses have been presented as data points in Fig. 20 for every 1/8th flat face curve of Fig. 18. These average stresses have been calculated according to Eq. (3) substituting $\sigma_{LB} = 0$. Without the bending component, the effect of the term σ_{LM} remains in integration because of the absolute value. By fitting a polynomial to these average stresses, the following equation is obtained:

$$\sigma_{LM,\mu,Flat}(f_y) = \begin{cases} 2.158 \bullet 10^{-7} \bullet f_y^{\,2} - 4.194 \bullet 10^{-4} \bullet f_y + 0.242, for f_y \le 970\,MPa \\ 0.038, for f_y > 970\,MPa \quad [1/f_y] \end{cases} \tag{8}$$

where f_y is the yield stress of the flat region in MPa. The polynomial of Eq. (8) is plotted in Fig. 20, and it models the mean membrane residual stress $\sigma_{LM,\mu,Flat}$. By fitting the polynomial in real stress space (instead of relative) yields to curve $\sigma_{LM,s\text{-}space}$ shown also in the figure. This curve provides slightly higher stresses for steel grades S350 and below. To prevent a small but illogical rise of membrane residual stress after $f_y =$

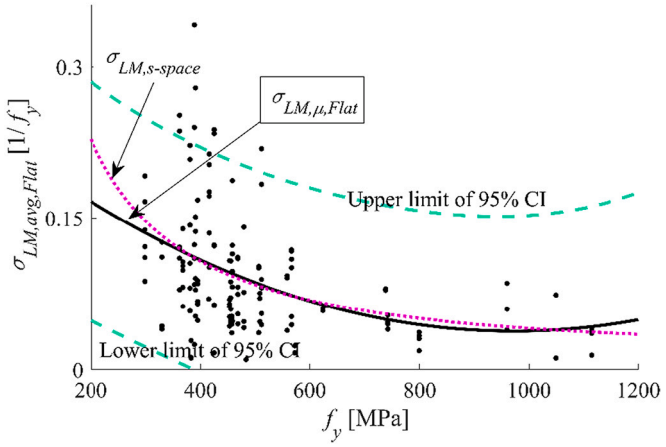

Fig. 20. Average longitudinal membrane residual stresses in the function of yield stress and polynomial fit $\sigma_{LM,\mu,Flat}$.

970 MPa, it is suggested that the polynomial of Eq. (8) is used until $f_y \le$ 970 MPa, after which membrane residual stress is assumed constant, 0.038.

Eq. (8) yields residual stresses of 0.12–0.04 for steels S350-S900. It should be noted that these stresses are the average membrane stresses in the flat region. When the membrane stresses are modelled according to χ_{LM} of KH, the residual stress value at MP or NC is twice the value given by Eq. (8), because of the triangular geometry of χ_{LM} (see Fig. 4). Multiplying these values by the factor 2 results in 0.24 (S350) and 0.08 (S900). In model KH, σ_{LM} is 0.09 at MP in the case of S350 steel, and in DB σ_{LM} is 0.17. Hence, Eq. (8) yields higher magnitudes for NSS and lower magnitudes for HSS than DB. The mean of data points in Fig. 20 is 0.09 and the coefficient of variation is 0.66. The coefficient of determination for the polynomial of Eq. (8) is 0.17.

4.2.7. Statistical properties of σ_{LM}

A normalized histogram of the error term $\sigma_{LM,\Delta,Flat}$ is shown in Fig. 14 (e) with KDE, Normal, and Johnson SB density functions. The mean of $\sigma_{LM,\Delta,Flat}$ is 0 and the sample STD is 0.056. CDF's are shown in Fig. 14(f), and Johnson SB corresponds better to Empirical than Normal. A Log-normal distribution has been assumed for the membrane component in the previous study [37], with the mean of 0.1 and STD of 0.08. However, the Log-normal distribution is for positive values only. If the distribution of $\sigma_{LM,\Delta,Flat}$ is translated adding a mean value of 0.11 such that all values are positive, a Log-normal distribution can be fitted with a mean of 0.11 and STD of 0.07. Multiplication of STD 0.07 by 2 (triangular geometry) results in 0.14, which is greater than the value presented in the literature (0.08). In the case of the translated distribution, Log-normal follows Empirical CDF better than Normal around the lower tail region. In the upper tail region, however, Log-normal is not so accurate as Normal resulting in remarkably higher magnitudes than Empirical, being conservative. Johnson SB has the best overall correspondence to the Empirical. Hence, the simplest i.e. Normal distribution and the most accurate i.e. Johnson SB distribution are considered in this study.

4.3. Transversal residual stresses

Transversal residual stress measurements σ_T are presented in Fig. 21 for the outer and inner surfaces. The data set consisted a total of 122 outer and 23 inner surface measurements. Transversal stresses have not been studied as extensively as longitudinal in the literature, hence transversal outer surface measurements belonged to 11 and inner surface only to 2 different specimens. Due to the small sample size, the statistical representativeness of the measurements is limited. Therefore, the transversal component has not been analyzed as detailed as the

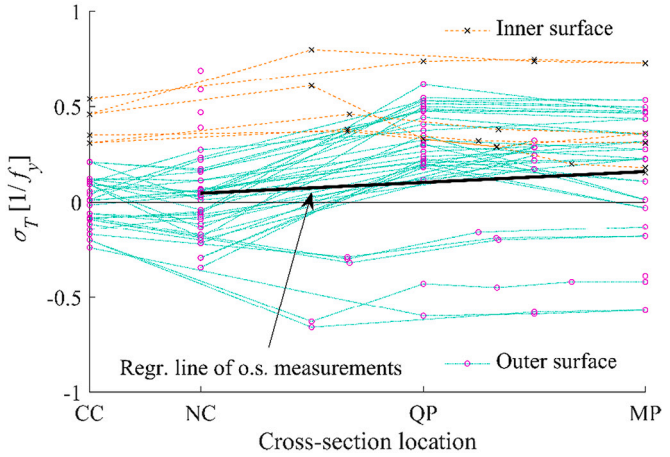

Fig. 21. Transversal residual stress measurements at outer and inner surfaces (each 1/8th face connected with lines).

longitudinal.

4.3.1. χ_{TB} for transversal bending component

The distribution of χ_{TB} is determined from the variation of σ_{TB} along the cross-section perimeter. Both compressive and tensile stresses are measured at the outer surface according to Fig. 21. A regression line is shown in the figure for all outer surface measurements from MP to NC. The slope of the regression line is positive, hence transversal stresses increase from NC to MP on average. However, due to the high variation among the connecting lines, χ_{TB} does not have a universal shape. Therefore, it seems reasonable to assume χ_{TB} as a simple straight horizontal line according to the model KH of Fig. 5.

Model KH uses the same χ_{TB} for both the corner and flat parts. According to a common assumption, the effect of transversal residual stresses on column strength is minor compared to longitudinal stresses. In addition, the corner region represents only a small portion of the whole cross-section area. Therefore, transversal stresses in the corner region probably are of secondary importance, and the model KH is adopted also for the corner due to the simplicity of the model.

4.3.2. Magnitude σ_{TB} for transversal bending component

Average transversal residual stresses have been presented as data points in Fig. 22 for every 1/8th flat face. These average stresses have been calculated according to Eq. (3) substituting $\sigma_{LB} = \sigma_{TB}$ and $\sigma_{LM} = \sigma_{TM} = 0$. It is assumed that the average transversal residual stress directly represents the magnitude of transversal bending component σ_{TB} at the outer surface. This assumption holds if the transversal membrane component σ_{TM} is zero. According to Ma et al. [18], the magnitude of σ_{TM} is low compared to the magnitude of σ_{TB}. Additionally, nonzero σ_{TM} would add a third dimension, i.e. variation along the length of a member, to the residual stress model. The third dimension would be needed because residual stresses are self-equilibrating stresses and are in balance without the application of external load. Therefore, nonzero transversal membrane component at some longitudinal axis location must be counteracted with opposite force at some other location, such that zero net membrane force requirement is satisfied. The third dimension would decrease the practicability of the model significantly. Thus, because of the secondary importance of the σ_{TM} and for the practicability, σ_{TM} is assumed to be zero such as in model KH.

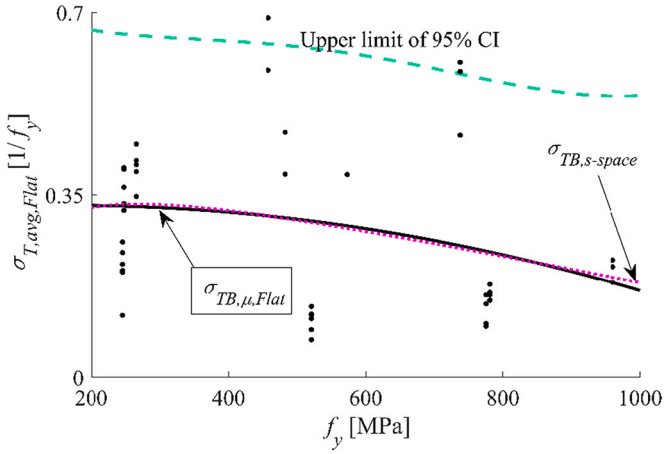

Fig. 22. Average transversal residual stresses at the outer surface in the function of yield stress and polynomial fit $\sigma_{TB,\mu,Flat}$.

By fitting a second-order polynomial to the average stresses of Fig. 22 the following polynomial is obtained:

$$\sigma_{TB,\mu,Flat}(f_y) = \begin{cases} -2.339 \bullet 10^{-7} \bullet f_y^2 + 7.613 \bullet 10^{-5} \bullet f_y + 0.324, for f_y \le 960 MPa \\ 0.181, for f_y > 960 MPa \end{cases} \left[1/f_y\right] \quad (9)$$

where f_y is the yield stress of the flat region in MPa. Due to the small sample size, the highest f_y of the measured specimens was 960 MPa. Therefore Eq. (9) is not valid for yield stresses above 960 MPa. In the case of f_y higher than 960 MPa, it is recommended to calculate $\sigma_{TB,\mu,Flat}$ assuming $f_y = 960$ MPa in the equation.

The polynomial of Eq. (9) is plotted in Fig. 22, and it models the mean transversal bending residual stress level at surfaces. It should be noted that the polynomial is based only on a few samples, i.e. considerable uncertainty exists in the polynomial shape. However, despite the small sample size, fitted polynomial $\sigma_{TB,\mu,Flat}$ yields to the similar shape as $\sigma_{LB,\mu,Flat}$, supporting the view that the modelled nonlinear dependence truly exists between residual stresses and the yield stress. If the polynomial is fitted in a real stress space, curve $\sigma_{TB,s\text{-}space}$ shown as a dotted line in Fig. 22 is obtained. This polynomial yields equal stress magnitudes in practice. Eq. (9) provides a magnitude of 0.32 for S350, which is about twice the magnitude of the model KH (0.17, see Fig. 5). The mean of data points in Fig. 22 is 0.29 and the coefficient of variation is 0.56. The coefficient of determination for the polynomial of Eq. (9) is 0.08. The low value for the coefficient of determination is expected, because the scatter of data points in Fig. 22 is huge, and the fitted polynomial resembles a horizontal line, i.e. the line that Eq. (9) is compared to.

4.3.3. Statistical properties of σ_{TB}

The normalized histogram and PDF's are shown in Fig. 14 (g) for the error term $\sigma_{TB,\Delta,Flat}$. Mean of $\sigma_{TB,\Delta,Flat}$ is 0 and sample STD 0.16. Empirical, Normal and Johnson CDF's are shown in Fig. 14 (h). The distribution is slightly bimodal, which causes some differences between Empirical and fitted CDF's. The sample size of the transversal stresses was rather low, i.e. Empirical CDF may not represent the true characteristics of the whole population. Thus, by considering the uncertainty in Empirical CDF and the high variation of the residual stresses in general, the differences between CDF's seem relatively minor. Hence the usage of Normal and Johnson distributions for $\sigma_{TB,\Delta,Flat}$ seem acceptable. The normal distribution has been employed for the transversal component in the previous study [37], with a mean of 0.5 and a standard deviation of 0.04.

4.3.4. Through-thickness distribution of σ_{TB}

Transversal residual stress measurements that contain two or more measurements at the same cross-sectional location are presented in Fig. 23. Results of Ma et al. have been included in the through-thickness data even they do not contain internal measurements because they are the only transversal measurements from the inner surface. Transversal through-thickness data is scarce, and it consists only of 3 different studies with a total of 5 different specimens.

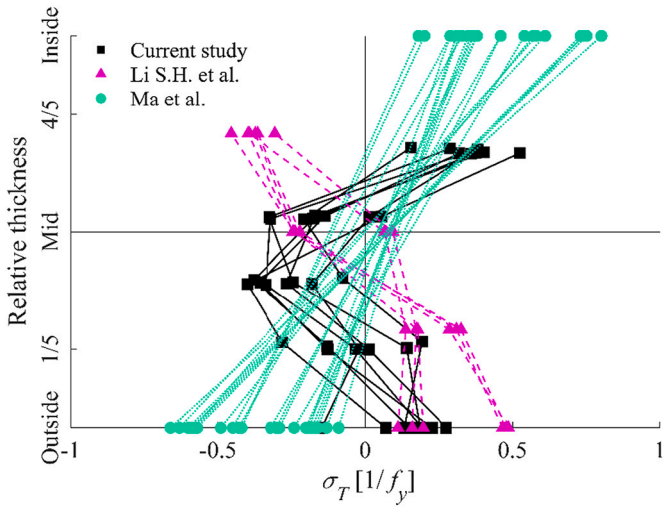

Fig. 23. Transversal residual stress data that contains two or more measurements from the same cross-sectional location.

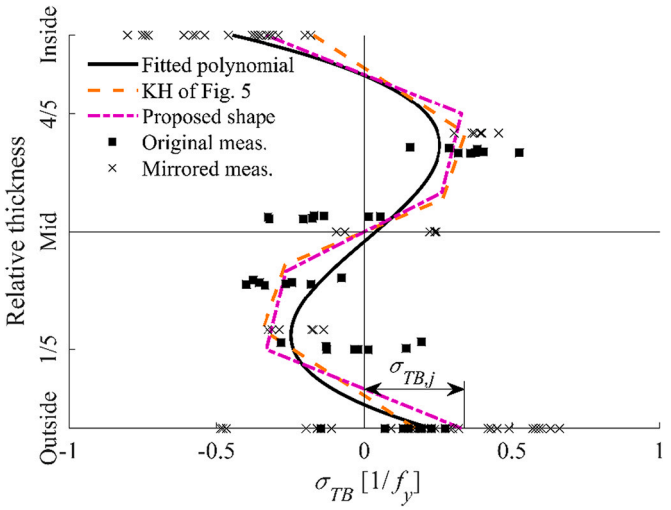

Fig. 24. Comparison of through-thickness shapes for σ_{TB}.

According to model KH shown in Fig. 5, the transversal bending component has a zigzag distribution through the thickness. A similar zigzag pattern may be seen in Fig. 23, although the measurements of Li S.H. et al. and Ma et al. seem to produce opposite σ_T readings than KH. Yao et al. [39] developed a finite element-based calculation model for determining the distribution of residual stresses in CFRHS. The model resulted in a similar kind of zigzag pattern in transversal stresses as KH. However, the zigzag pattern had opposite stress readings, i.e. mirrored shape at corner regions compared to flat regions. Ma et al. [18] measured tensile stresses at the inner surface and compressive at the outer, which are opposite both to KH and most of the results of Yao et al. Conflicts between the measurements of Fig. 23, model KH and results of Yao et al. suggest that the zigzag pattern can be in either direction depending on the deformation history of a member.

Steel materials are usually modelled as von Mises materials, in which the deviatoric stresses determine whether the material yields or not. If the transversal component in some specific through-thickness location has the same sign as the longitudinal component, deviatoric stresses become lower compared to the case where the components would have opposite signs. Hence, the direction of the zigzag pattern affects the plasticization of the material. The impact of this issue is estimated in the parametric study.

The through-thickness distribution cannot be determined appropriately from the conflicting measurements of Fig. 23. However, when the results of Li S.H. et al. and Ma et al. are mirrored along the vertical axis and presented with the results of the current study, data points form a zigzag through-thickness shape as shown in Fig. 24. By fitting a third-order polynomial to this data, a curve that matches remarkably well to the KH is obtained as shown in the figure.

In addition, a new through-thickness distribution is proposed and plotted to the figure. The proposed shape is obtained by slightly modifying the model KH according to the following steps: (1) Residual stress magnitude at the surfaces is the mean of the polynomial's outer and inner surface absolute values. (2) The maximum and minimum values inside the thickness have been selected to be the same as at surfaces, which is conservative compared to the polynomial. (3) Ratio between the stress magnitudes at relative thicknesses of 0.25 and 0.42 as well as of 0.75 and 0.58 is 0.27/0.34 = 0.8 in KH (see Fig. 5). The same ratio fits the polynomial conservatively, hence it is adopted to the proposed model. (4) The proposed shape is determined at the same relative thicknesses as the longitudinal bending model such that through-thickness layers of components are consistent.

4.4. The proposed probabilistic model

The proposed probabilistic residual stress model is presented in Fig. 25 for steel grades up to S960. Residual stress values in Fig. 25 for a probabilistic study are obtained by summing up the mean value μ and the sampled error term Δ according to Eq. (7). Parameters μ and Δ are calculated according to the statistics of Table 5. The table contains two optional distributions for the error terms. Although Johnson's distributions are more accurate, the Normal distributions follow Empirical CDFs also well as shown in Fig. 14. Hence, Normal distributions are recommended due to simplicity. If $\sigma_{LB,Corner}$ is assumed to fully correlate with $\sigma_{LB,Flat}$, then $\sigma_{LB,\mu,Corner}$ is calculated according to Eq. (6) and no error term is needed, i.e. $\sigma_{LB,\Delta,Corner} = 0$. Dependence between the components can be considered using Pearson's correlation coefficients, which are presented in Table 6. A strong correlation is observed between the components $\sigma_{LB,Flat}$ and $\sigma_{LB,Corner}$ and between $\sigma_{LB,Flat}$ and $\sigma_{TB,Flat}$. The residual stress distribution along the cross-sectional perimeter is obtained by multiplying the through-thickness distributions with the corresponding distribution factors χ according to Eqs. (1) and (2).

The following were assumed in deriving the proposed model:

- The mean residual stress level is dependent on the yield stress: To keep the model practical, magnitudes of residual stresses are only functions of the yield stress, even other explanatory variables have also been suggested to affect residual stresses (see Section 4.2.2).
- Statistical distribution of the residual stress is independent of the yield stress: Sample size for HSS measurements is too low to develop yield stress-specific error terms (see Section 4.2.3).
- Heat affected zone caused by the longitudinal welding has no impact on the model: Measurements obtained from the weld location are excluded from the used data set when deriving the residual stress model. The model is assumed to be the same for all flanges and webs of the CFRHS member.
- Shear stresses τ_{xy}, τ_{xz}, τ_{yz} and normal stress σ_z shown in Fig. 1 are zero: The effect of these components on the global buckling capacity is assumed to be insignificant.
- The transversal through-thickness membrane component σ_{TM} is zero: The magnitude of σ_{TM} is low compared to σ_{TB} and consideration of σ_{TM} would add a third dimension to the model, thus decreasing the practicability of the model (see Section 4.3.2).
- The longitudinal membrane component σ_{LM} is zero in the corner region: σ_{LM} has only a minor effect on the global buckling capacity of the CFRHS member and the corner region represents a small portion of the whole cross-sectional area, hence σ_{LM} in the corner region is considered insignificant (see Section 4.2.5).

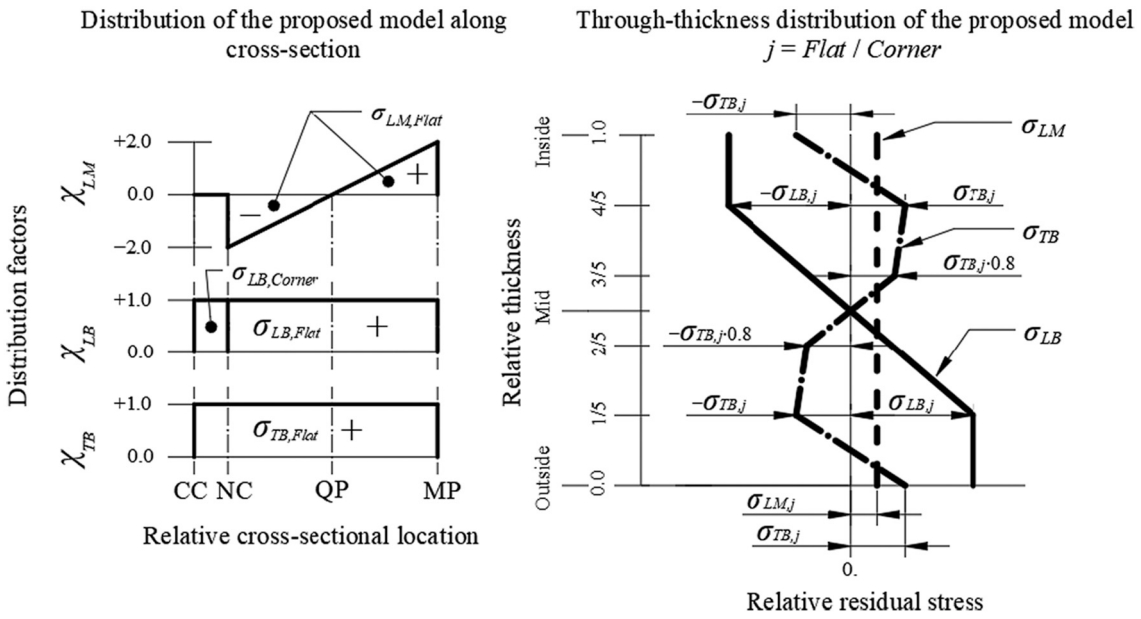

Fig. 25. Residual stress distributions of the proposed model.

Table 6
Pearson's correlation coefficients between components.

	$\sigma_{LB,Flat}$	$\sigma_{LB,Corner}$	$\sigma_{LM,Flat}$	$\sigma_{TB,Flat}$
$\sigma_{LB,Flat}$	1.0	0.80	−0.04	0.76
$\sigma_{LB,Corner}$	symm.	1.0	−0.19	0.69
$\sigma_{LM,Flat}$	symm.	symm.	1.0	0.32
$\sigma_{TB,Flat}$	symm.	symm.	symm.	1.0

It should be noted that the model is presented only for a 1/8th cross-section face because the model is symmetrical with respect to the axes 1–1 and 2–2 of Fig. 3. This is justified since the average bending residual stress magnitudes between 1/8th faces of the same specimens are highly correlated with each other, Pearson's correlation coefficients being 0.73 for longitudinal and 0.96 for transversal bending components.

It should also be noted that because the individual 1/8th faces are investigated instead of whole cross-sections, the specimens with multiple faces measured gain more weight in regression analysis than specimens with fewer faces measured. Therefore, regression curves were also fitted based on the whole specimens, and this led almost to identical results in general for longitudinal components. At maximum, the regression curves for whole specimens gave about 5% higher output residual stresses (not relative residual stresses) for $\sigma_{LB,\mu,Flat}$ and 14% higher for $\sigma_{LB,\mu,Corner}$. For $\sigma_{LM,\mu,Flat}$, the regression curve of the whole specimens gave about 8% lower magnitudes. In the case of the transversal bending component, the regression curve of the whole specimens gave about 30% higher output residual stresses at maximum. This study considered every 1/8th face as an independent sample because the more the measurements from the specimen, the more reliable the result is, i.e. allowing weight according to reliability is reasonable.

5. Parametric study for modelling simplifications

A parametric study has been carried out for evaluating the effects of modelling simplifications on the global buckling capacity of a compressed steel member. According to Somodi and Kövesdi [13], residual stresses have the highest impact on the global buckling capacity of the S700 column at the non-dimensional slenderness around 1.2. Therefore, a pinned cold-formed column with a cross-section size of 150x150x8, buckling length L of 3.6 m, and steel grade of S700 was chosen for the evaluation, such that the non-dimensional slenderness corresponds to 1.2.

5.1. FE model

The parametric study has been conducted with a commercial FEM package Abaqus [40]. Geometry was modelled using shell elements of type S4R, with Simpson's integration having 11 integration points through the material thickness. According to mesh convergence studies the target element size of 12.5 (width) x 12.5 (height) x 25.0 (length) mm was suitable. Boundary conditions were modelled by coupling the nodes of the cross-section at the top and bottom ends to boundary nodes with multipoint constraints, see Fig. 26. All other than a rotational degree of freedom in the buckling direction were constrained to be zero at the bottom boundary node. At the top boundary node, all other than the rotational degree of freedom in the buckling direction and the translational degree of freedom in the longitudinal axis direction were constrained to be zero, thus allowing the column to buckle. Displacement controlled load compressing the column along the longitudinal axis was assigned to the top boundary node.

Out-of-straightness i.e. bow imperfection in the form of the lowest buckling mode (sinusoidal half-wave) was considered as an initial geometrical imperfection in the buckling direction. Analyses were

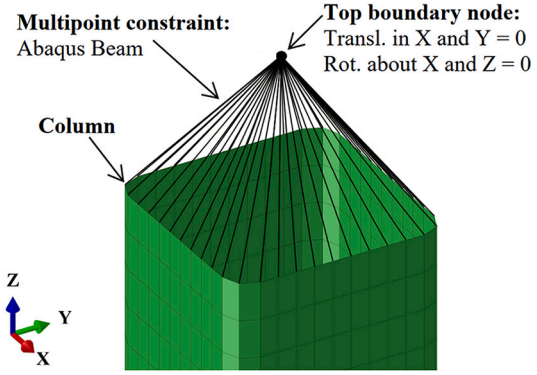

Fig. 26. Boundary conditions at the top boundary node.

Table 7
Material parameters for the two-stage Ramberg-Osgood model [42].

Parameter	Description	Flat	Corner
f_y	Tensile yield strength (0.2% proof stress)	749 MPa	824 MPa
f_u	Ultimate tensile strength	829 MPa	870 MPa
$\sigma_{0.05}$	0.05% proof stress	644 MPa	708 MPa
E	Elastic modulus	210 GPa	
ν	Poisson's ratio	0.3	

carried out with two magnitudes of bow imperfections: L/1000 which is the allowed geometrical bow imperfection according to EN 1090–2 [41] and employed when designing with advanced methods, and L/7937 which has been employed in the reliability studies when developing such methods [3].

The material was modelled according to von Mises yield surface and associated plastic flow with isotropic hardening. The stress-strain curve of the material in the parametric study was modelled according to a two-stage Ramberg-Osgood model of Gardner and Yun [42] up to the ultimate tensile strength, after which the yield plateau was assumed constant. Chosen parameters for the material model are shown in Table 7. Stress parameters of the flat region in the table were determined such that they fitted well to the experimentally measured stress-strain curve. The material in the corner region is hardened compared to the flat region [18], thus enhanced material parameters were used for corner material.

Longitudinal bending residual stress at corners was assumed to fully correlate with the flat region according to Eq. (6). Assuming error term $\Delta = 0$, the proposed model yields to the mean values of $\sigma_{LB,Flat} = 0.63$, $\sigma_{LB,Corner} = 0.50$, $\sigma_{LM,Flat} = 0.05$, and $\sigma_{TB,Flat} = 0.25$ for the yield stress of the flat region presented in Table 7. If the error term Δ is taken into account, e.g. determining the 95% fractile value, the model yields the value of $\sigma_{LB,Flat} = 0.97$ in the case of Normal distribution. It should be noted that if $\sigma_{LB,\mu,Corner}$ is calculated according to Eq. (5), i.e. without full correlation to $\sigma_{LB,Flat}$, the $\sigma_{LB,\mu,Corner}$ is determined using the yield stress of the flat region and not the enhanced corner yield stress. Relative residual stresses are finally transformed to real residual stresses by multiplying the relative stresses with the yield strength of the flat region. For example, $\sigma_{LB,Corner}$ becomes 0.50•749 MPa = 375 MPa.

Residual stresses were modelled as initial stresses and equivalent plastic strains by the Abaqus Fortran subroutines SIGINI and HARDINI. Initial stresses were incorporated directly to integration points of the shell element. Corresponding equivalent plastic strains were determined from the Von Mises stresses caused by the longitudinal and transversal initial stresses. Residual stresses were applied to the calculation model in a preliminary static analysis step using Newton's method. Subsequently, the actual buckling analysis was performed by the arc-length method.

The modelling method was validated against the experimental global buckling tests conducted for HSS sections by Somodi and Kövesdi [13]. FE -model gave 7% smaller capacities than the experimental ones on average. Differing results between FE-models and experimental tests were caused by conservative modelling assumptions, which were not related to residual stresses apart from one cause: According to [43,44] the stress-strain curves obtained from the tensile coupon tests may include already some effects of the longitudinal bending residual stress, thus longitudinal bending component may be accounted twice to some extent. This is since the material coupon is curved after extracting it due to the release of the bending residual stress. Then, the coupon is straightened when fastening it to a testing machine, and the longitudinal bending residual stress is reintroduced to the coupon. However, despite the differences between the FEM and validation models, the modelling technique had an adequate accuracy for this study.

5.2. Results of the parametric study

Effects of modelling simplifications are evaluated by comparing the buckling capacities of the reference mean model R_{Mean} to modified models $R_{Modified}$. The mean model R_{Mean} was modelled according to the proposed residual stress model of Section 4.4 with the mean residual stress values. A total of 11 modified models $R_{Modified}$ were studied for differing assumptions, and Table 8 describes the studied cases and their relative buckling capacities in the form of $R_{Modified}$ / R_{Mean}. In modified models, only the described component-specific feature was modified, retaining the rest of the properties as in model R_{Mean}.

Similar relative capacities between the differing bow imperfections in Table 8 indicate that the parametric study is not sensitive to the used bow imperfection. Case no. 1 is a calculation without the residual stress components, which results in about 16% higher buckling capacities. Cases 2, 6 and 9 study capacities without individual components, and capacities are about 14% (σ_{LB}), 0.3% (σ_{LM}), and 2% (σ_{TB}) higher. Hence, the σ_{LB} has a major impact on the buckling capacity, whereas σ_{TB} has a clear but rather minor and σ_{LM} almost negligible effect. Cases 3, 7 and 10 study the sensitivity of the capacity to the error term Δ having the magnitudes according to the 95% fractile value of the proposed statistical model. This decreases capacities about 7% (σ_{LB}), 0.8% (σ_{LM}) and 1.7% (σ_{TB}). The results above suggest that σ_{LB} and σ_{TB} have a clear impact on the capacity such that it is recommended to consider these components in reliability studies. In the practical use of advanced methods with HSS members, it may be justified to disregard the σ_{TB}. In the case of the σ_{LM}, it may be justified to disregard it both in the reliability studies and practical use.

Cases 4 and 8 study the effects of the shapes of χ_{LB} and χ_{LM} on the capacity. The proposed model uses a simplified uniform distribution of χ_{LB} shown in Fig. 25. However, according to Fig. 9, residual stresses have various shapes along the cross-section perimeter, and the regression

Table 8
Calculation results of the parametric study.

Modified component	Case	Modification	Relative capacity (%)	
			L/1000	L/7937
$\sigma_{LB},\sigma_{LM},\sigma_{TB}$	1	Without residual stress components	114.7	117.5
σ_{LB}	2	Without the component	112.5	115.0
	3	Magnitude according to 95% fractile value	93.0	92.6
χ_{LB}	4	The slope of χ_{LB} according to Fig. 10(b), case 30 ≤ B/t. (χ_{LB} = 0.75 at MP, 1.25 at NC)	100.0	100.0
Through-thickness of σ_{LB}	5	Linear through-thickness distribution	103.9	104.3
σ_{LM}	6	Without the component	100.3	100.3
	7	Magnitude according to 95% fractile value	99.1	99.3
χ_{LM}	8	Linearly increasing χ_{LM} from MP to NC, −2.0 at MP, +2.0 at NC.	100.4	100.4
σ_{TB}	9	Without the component	101.5	101.7
	10	Magnitude according to 95% fractile value	98.3	98.3
Through-thickness of σ_{TB}	11	Mirrored through-thickness zigzag distribution along mid-thickness	102.5	103.2

lines shown in Fig. 10 (b) have varying slopes depending on the B/t-ratio. Case 4 modifies the χ_{LB} such that it corresponds to case $30 \leq$ B/t of Fig. 10(b). Surprisingly, this modification does not affect capacity within the used decimals. Hence, it seems valid to model χ_{LB} as a simple uniform distribution. In case 8, a mirrored χ_{LM} along the zero horizontal axis of Fig. 25 is used such that χ_{LM} has the opposite slope direction than the regression lines of Fig. 19. This modification is studied because, for some individual members, the σ_{LM} distribution does not correspond to regression lines. This modification has only a minor effect, 0.4%, on the capacity. Because capacity increases due to the modification, the slope direction of χ_{LM} in the proposed model seems conservative.

Cases 5 and 11 study the effects of the through-thickness distributions of σ_{LB} and σ_{TB} on the capacity. In case 5, a linear through-thickness distribution, i.e. distribution almost like for "Mid plate" in Fig. 16, is used for the σ_{LB}. This modification leads to an over 4% increase in capacity. Because the linear distribution is unconservative for near corner and corner regions (see Fig. 16), and using it leads remarkably higher capacities, it is recommended to use the proposed piecewise linear distribution shown in Fig. 25. The proposed piecewise linear distribution can be perceived as "an average" of the model DB and the linear distribution: In DB, the σ_{LB} remains constant till 1/3 material thickness (see Fig. 2), whereas in the proposed model only till 1/5 thickness. This is justified because measurements in the dataset, which have been obtained by the sectioning method, assume the linear bending distribution without scaling down the measured surface strain readings (see Section 4.1). In case 11, the through-thickness zig-zag distribution of Fig. 25 is mirrored along the mid-thickness. This modification increases the capacity by about 3%. A probable reason for this behaviour is that with the mirrored zig-zag distribution, the transversal and longitudinal bending components have the same sign most of the material thickness, thus decreasing the von Mises stresses compared to the case with different signs. The proposed model yields conservative values with the chosen through-thickness distribution of the σ_{TB}. Naturally, the conservatively chosen direction may be one source of an error between validation and experimental models.

It should be noted that the slenderness of the evaluated structure was chosen such that the structure is very sensitive to residual stresses. In the case of some other slenderness, the evaluated modifications probably have smaller impacts. On the other hand, the evaluation was carried out only for the steel grade S700, and with a different grade, results may also differ.

6. Conclusions

This study proposed a residual stress model, which is suitable for cold-formed rectangular hollow sections made of steel grades up to S960 by the continuous forming method. The model determines longitudinal and transversal residual stresses in the through-thickness direction and around the cross-section perimeter. The model can be used in advanced design methods and reliability studies, which require that residual stresses are incorporated into the calculation model.

The proposed model was based on extensive data analysis, in which two existing residual stress models by Davison and Birkemoe and Key and Hancock were evaluated for a data set. The data set contained residual stress measurements found from the literature and supplemented with new measurements performed by the authors on S700 hollow sections. The used measuring method was the X-ray diffraction method, which enabled the measurement of both longitudinal and transversal residual stress components. As a result of the evaluation, a new model was proposed for the residual stresses, which combines the best matching features of the existing models with slight modifications: The longitudinal through-thickness distribution of the proposed model was based on the model Davison and Birkemoe and the remaining features were based on the model Key and Hancock. Probabilistic information of the proposed model was determined from the data set.

Development of the proposed model involved simplifications. The effects of these simplifications were studied on the global buckling capacity of a steel member (grade S700) in a parametric study. Results of the parametric study indicated that simplifications made had a slightly conservative or insignificant effect on the capacity. Longitudinal and transversal bending components had a clear impact on the capacity such that it is recommended to consider these components in reliability studies: Without the longitudinal bending component capacity was about 14% higher and without the transversal bending component about 2% higher. In the practical use of advanced methods, it may be justified to disregard the transversal bending component. In the case without the longitudinal membrane component, capacity was only 0.3% higher. Therefore, it may be justified to disregard it both in the reliability studies and practical use.

Declaration of Competing Interest

The authors declare that they have no known competing financial interests or personal relationships that could have appeared to influence the work reported in this paper.

Acknowledgements

This research was funded by the Doctoral School of Industry Innovations at Tampere University and SSAB Europe. The funding and support are gratefully acknowledged.

References

[1] R.D. Ziemian, Guide to Stability Design Criteria for Metal Structures, Hoboken, N.J, John Wiley & Sons, 2010.
[2] SFS-EN 1993-1-1 + AC, Eurocode 3: Design of steel structures. Part 1–1: general rules and rules for buildings, 2005.
[3] W. Liu, H. Zhang, K. Rasmussen, System reliability-based direct design method for space frames with cold–formed steel hollow sections, Eng. Struct. 166 (2018) 79–92.
[4] T.A. Davison, P.C. Birkemoe, Column behaviour of cold-formed hollow structural steel shapes. Canadian journal of civil engineering, Can. J. Civ. Eng. 10 (1983) 125–141.
[5] P.W. Key, G.J. Hancock, A theoretical investigation of the column behaviour of cold-formed square hollow sections, Thin-Walled Struct. 16 (1993) 31–64.
[6] L. Tong, G. Hou, Y. Chen, F. Zhou, K. Shen, A. Yang, Experimental investigation on longitudinal residual stresses for cold-formed thick-walled square hollow sections, J. Constr. Steel Res. 73 (2012) 105–116.
[7] B. Somodi, B. Kövesdi, Residual stress measurements on cold-formed HSS hollow section columns, J. Constr. Steel Res. 128 (2017) 706–720.
[8] EN 1993-1-5, Eurocode 3 - Design of steel structures - Part 1–5: Plated structural elements, 2006.
[9] W. Ramberg, W.R. Osgood, Description of Stress-Strain Curves by Three Parameters, 1943.
[10] G. Shi, X. Zhu, H. Ban, Material properties and partial factors for resistance of high-strength steels in China, J. Constr. Steel Res. 121 (2016) 65–79.
[11] H. Ban, G. Shi, Y. Shi, M.A. Bradford, Experimental investigation of the overall buckling behaviour of 960MPa high strength steel columns, J. Constr. Steel Res. 88 (2013) 256–266.
[12] B. Somodi, B. Kövesdi, Flexural buckling resistance of welded HSS box section members, Thin-Walled Struct. 119 (2017) 266–281.
[13] B. Somodi, B. Kövesdi, Flexural buckling resistance of cold-formed HSS hollow section members, J. Constr. Steel Res. 128 (2017) 179–192.
[14] H. Fang, T. Chan, B. Young, Structural performance of cold-formed high strength steel tubular columns, Eng. Struct. 177 (2018) 473–488.
[15] S.H. Li, G. Zeng, Y.F. Ma, Y.J. Guo, X.M. Lai, Residual stresses in roll-formed square hollow sections, Thin-Walled Struct. 47 (2009) 505–513.
[16] L. Gardner, N. Saari, F. Wang, Comparative experimental study of hot-rolled and cold-formed rectangular hollow sections, Thin-Walled Struct. 48 (2010) 495–507.
[17] M. Sun, J.A. Packer, Direct-formed and continuous-formed rectangular hollow sections — comparison of static properties, J. Constr. Steel Res. 92 (2014) 67–78.
[18] J. Ma, T. Chan, B. Young, Material properties and residual stresses of cold-formed high strength steel hollow sections, J. Constr. Steel Res. 109 (2015) 152–165.
[19] X. Zhang, S. Liu, M. Zhao, S. Chiew, Comparative experimental study of hot-formed, hot-finished and cold-formed rectangular hollow sections, Case Stud. in Struct. Eng. 6 (2016) 115–129.
[20] M. Sun, Z. Ma, Effects of heat-treatment and hot-dip galvanizing on mechanical properties of RHS, J. Constr. Steel Res. 153 (2019) 603–617.
[21] R.M. Sully, G.J. Hancock, Behavior of cold-formed SHS beam-columns, J. Struct. Eng. (New York, N.Y.) 122 (1996) 326–336.

[22] Y. Sun, V. Luzin, W.J.T. Daniel, P.A. Meehan, M. Zhang, S. Ding, Development of the slope cutting method for determining the residual stresses in roll formed products, Measurement 100 (2017) 26–35.
[23] G. Li, Y. Li, J. Xu, X. Cao, Experimental investigation on the longitudinal residual stress of cold-formed thick-walled SHS and RHS steel tubes, Thin-Walled Struct. 138 (2019) 473–484.
[24] K. Tayyebi, M. Sun, K. Karimi, Residual stresses of heat-treated and hot-dip galvanized RHS cold-formed by different methods, J. Constr. Steel Res. 169 (2020), 106071.
[25] Hayeck Marielle, Development of a New Design Method for Steel Hollow Section Members Resistance (Ph.D. thesis), Universite De Liege, 2016.
[26] T. Jokiaho, Residual Stress, Microstructure and Cracking Characteristics of Flame Cut Thick Steel Plates Towards Optimized Flame Cutting Practices, 2019.
[27] EN ISO 6892-1:2019, Metallic materials. Tensile testing. Part 1: Method of test at room temperature, 2019.
[28] R.L. Peng, R. Alkaisee, Influence of Layer Removal Methods in Residual Stress Profiling of a Shot Peened Steel Using X-Ray Diffraction 996, 2014, pp. 175–180.
[29] EN 15305: Non-destructive Testing Method for Residual Stress analysis by X-ray Diffraction 2008.
[30] B.D. Cullity, Elements of x-ray diffraction, Reading, Mass. [u.a.], Addison-Wesley, 1967.
[31] M. Fitzpatrick, A. Fry, F. Holdway, J. Kandil, J. Shackleton, L. Suominen, Determination of residual stresses by X-ray diffraction, Meas. Good Practice Guide 52 (2005).
[32] S. Mehtonen, V. Kesti, J. Mourujärvi, A. Kaijalainen, Effect of Thermomechanical Processing on the Microstructure, Texture and Impact Toughness of Two 700 MPa Strength Class Structural Steels, 2016.
[33] A. Kaijalainen, J. Mourujärvi, J. Tulonen, P. Steen, J. Kömi, Effect of direct quenching on the mechanical properties of cold formed S500 rectangular hollow section, Procedia manufacturing 50 (2020) 777–783.
[34] A.W. Bowman, A. Azzalini, Applied Smoothing Techniques for Data Analysis, Oxford University Press, Oxford, 1997.
[35] N.L. Johnson, Systems of frequency curves generated by methods of translation, Biometrika 36 (1949) 149.
[36] D. Jones, Johnson curve toolbox, version 1.5.0.0, MATLAB Central File Exchange. (2021). https://www.mathworks.com/matlabcentral/fileexchange/46123-johnson-curve-toolbox. Retrieved April 7, 2021.
[37] H. Blum, Reliability-Based Design of Truss Structures by Advanced Analysis. Research Report R936, School of Civil Engineering, The University of Sydney, 2013.
[38] W. Liu, K.J.R. Rasmussen, H. Zhang, Modelling and probabilistic study of the residual stress of cold-formed hollow steel sections, Eng. Struct. 150 (2017) 986–995.
[39] Y. Yao, W. Quach, B. Young, Finite element-based method for residual stresses and plastic strains in cold-formed steel hollow sections, Eng. Struct. 188 (2019) 24–42.
[40] Dassault Systémes SIMULIA Corp. Abaqus R2019x.
[41] EN 1090–2, Execution of steel structures and aluminium structures. Part 2: Technical requirements for steel structures, 2018.
[42] L. Gardner, X. Yun, Description of stress-strain curves for cold-formed steels, Constr. Build. Mater. 189 (2018) 527–538.
[43] K.J.R. Rasmussen, G.J. Hancock, Design of Cold-Formed Stainless Steel Tubular Members. I: columns, J. Struct. Eng. (New York, N.Y.) 119 (1993) 2349–2367.
[44] M. Jandera, L. Gardner, J. Machacek, Residual stresses in cold-rolled stainless steel hollow sections, J. Constr. Steel Res. 64 (2008) 1255–1263.